

smoothEM: a new approach for the simultaneous assessment of smooth patterns and spikes

Huy Dang

Department of Statistics, The Pennsylvania State University, University Park, USA.

E-mail: hqd1@psu.edu

Marzia A. Cremona

Department of Operations and Decision Systems, Université Laval, Québec, Canada.

CHU de Québec – Université Laval Research Center, Québec, Canada

Francesca Chiaromonte

Department of Statistics, The Pennsylvania State University, University Park, USA.

Institute of Economics and EMbeDS, Sant'Anna School of Advanced Studies, Pisa, Italy.

Abstract. We consider functional data where an underlying smooth curve is composed not just with errors, but also with irregular spikes. We propose an approach that, combining regularized spline smoothing and an Expectation-Maximization algorithm, allows one to both identify spikes and estimate the smooth component. Imposing some assumptions on the error distribution, we prove consistency of EM estimates. Next, we demonstrate the performance of our proposal on finite samples and its robustness to assumptions violations through simulations. Finally, we apply our proposal to data on the annual heatwaves index in the US and on weekly electricity consumption in Ireland. In both datasets, we are able to characterize underlying smooth trends and to pinpoint irregular/extreme behaviors.

1. Introduction and Motivation

The past two decades have witnessed an increasing interest in functional data, where one or more variables are data varying over a continuum and often possessing additional structures of interest. The vast majority of past and current literature focuses on functional data obeying certain smoothness conditions (see, e.g., Ramsay and Silverman,

2007; Kokoszka and Reimherr, 2017). This kind of data can be effectively represented in low-dimension through basis functions (e.g., Fourier basis, spline basis or polynomial basis) and in the majority of applications a penalty is employed to ensure such representation – an approach commonly referred to as regularized smoothing (Yao and Lee, 2006; Xiao et al., 2016, 2018; Goldsmith et al., 2011; Wood, 2006). When functions have discontinuities and/or sporadic behaviors, wavelet bases are often preferred due to their ability to yield information about the functions at multiple resolutions (Nason, 2008). Wavelet-based methods, while characterized by estimation efficiency, can be ill-fitting for data where the true underlying trend is smooth, and where the sporadic discontinuities occur separately and/or independently from the underlying smooth trend. Somewhere in between, Descary and Panaretos (2019) consider functions with globally smooth components and rough components that are smooth only at local scales. More specifically, they work with a discretely observed function expressed as the sum of two uncorrelated components; $X(t) = Y(t) + W(t)$. $Y(t)$ is taken to be of finite rank and of smoothness class C^k ($k \geq 2$), while $W(t)$ is a locally highly variable but continuous function, assumed to be smooth at a much shorter time scale. While interesting in itself, this set-up is only an approximation for functions that contain true discontinuities, and are thus non-smooth at any scale.

In this article, we propose a different and more straightforward approach that represents discontinuities explicitly. Specifically, we consider a composite structure where data is generated from a smooth curve with additive errors – except at certain locations, where irregular behaviors occur in the form of additive spikes further superimposed to the “noisy curve”. In symbols, we are interested in data $(x_i, y_i)_{i=1}^n$ of the form

$$y_i = f(x_i) + \mu^* \cdot \mathbb{1}(x_i \in \mathbb{S}) + \epsilon_i \quad (1)$$

where $x_i, i = 1 \dots, n$ are locations in a domain (which we map in $[0, 1]$ without loss of generality); $f \in C^p[0, 1]$ is a smooth function with p continuous derivatives; \mathbb{S} is a random collection of intervals on $[0, 1]$ affected by spikes of size μ^* such that \mathbb{S} has probability measure $1 - \alpha^*$; $\mathbb{1}(x_i \in \mathbb{S}), i = 1 \dots, n$ is an indicator of spike occurrences; and $\epsilon_i, i = 1 \dots, n$ are independent random errors. Assuming a fixed design, our main goal is to capture the underlying curve and to identify the spikes, i.e. to estimate f and

the spike classification vector $\mathbb{1}_{\mathbb{S}} = (\mathbb{1}(x_i \in \mathbb{S}))_{i=1}^n$. This structure is rather common in applications. To provide some meaningful examples, we consider data on extreme temperatures (annual time series from the United States) and electricity consumption (weekly time series from Ireland). As we shall see, in both cases one can observe spikes occurring on top of smooth underlying trends, due, e.g., to sporadic abnormalities in weather conditions or occasional over-consumption of electricity. We are interested in producing reliable estimates of the underlying trends and in identifying the spikes, which can be analyzed (possibly using additional assumptions on their distribution) to gain insight into their frequency, location, magnitude and spread.

For these “spiky curves”, a simple application of regularized smoothing (e.g., with a spline basis) that does not account for the spikes can generate an inaccurate approximation of the underlying curve f in Equation (1), and also the approach of Descary and Panaretos (2019) does not allow for discontinuities of this kind. Instead, we propose a procedure that utilizes regularized smoothing splines, thus preserving assumptions about the smoothness of f , and combines them with an *Expectation-Maximization* (EM) algorithm (Dempster et al., 1977; Liu and Rubin, 1994; Louis, 1982; Meilijson, 1989; Meng and Rubin, 1993) which, under some conditions, allows us to identify the spikes. Because we preserve the smoothness of f , we are able to leverage existing results on penalized smoothing spline estimators (Claeskens et al., 2009; Eilers and Marx, 1996; Eilers et al., 2015; Hall and Opsomer, 2015; Kauermann et al., 2009; Wang et al., 2011; Xiao, 2019). The result is a good approximation of f , on par with that one would obtain in the absence of spikes.

With the additional assumption that errors are Gaussian, we rewrite Equation (1) as $y_i = f(x_i) + \xi_i$, where $\xi_i := \mu^* \cdot \mathbb{1}(x_i \in \mathbb{S}) + \epsilon_i$ can be modeled as a mixture of Gaussians; namely

$$\xi_i \sim \alpha^* N(0, \sigma^{*2}) + (1 - \alpha^*) N(\mu^*, \sigma^{*2}). \quad (2)$$

Thus, with probability $\alpha^* \in [0, 1]$, the departure from f is Gaussian with mean 0 and variance σ^{*2} , but with probability $(1 - \alpha^*)$ it is “spiked” by a scalar amount μ^* . In this setting, Maximum Likelihood estimates (MLE) of α^*, μ^* and σ^* could be obtained through the EM algorithm if the ξ_i ’s were observable. Previous work on EM convergence

often assumed that the only parameter to be estimated is μ^* , with both σ^{*2} and α^* taken as known; see for instance Wu et al. (2017) and Balakrishnan et al. (2017). Drawing inspiration from the latter, we study convergence when all parameters μ^*, σ^{*2} and α^* are unknown – proving that ν -strong concavity, Lipschitz smoothness and Gradient smoothness conditions hold for our Gaussian mixture model. Guarantees on the convergence rate are harder to establish when all three parameters are treated as unknown, but can in fact be provided if the “contamination” level α^* is taken as known. We use simulations to demonstrate the practical effectiveness of our approach notwithstanding this shortcoming in theoretical guarantees.

The remainder of this article is organized as follows. Section 2 provides background on smoothing splines and EM algorithm. Section 3 details our approach and the conditions under which it performs well. Section 4 provides convergence guarantees for the EM algorithm. Sections 5 and 6 demonstrate the performance of our proposal through simulations and real data analyses. Section 7 contains final remarks.

2. Technical background

In this section, we summarize relevant notions and results from existing literature. Some of the notation used here diverges from notation used in other parts of the text.

2.1. Smoothing splines

Suppose that the data $(x_i, y_i)_{i=1}^n$ are generated according to

$$y_i = f(x_i) + \epsilon_i \quad (3)$$

where $x_i \in [0, 1], i = 1, \dots, n$ are either fixed or random, and the ϵ_i 's represent white noise (independent and Gaussian random errors). Assuming that f has p continuous derivatives on $[0, 1]$, i.e. that $f \in C^p[0, 1]$, it is often of interest to approximate f from $(x_i, y_i)_{i=1}^n$. In a spline approximation (de Boor, 1978; Xiao, 2019) the estimator \hat{f} is restricted to lie in the space $\mathbb{S}_{m,t}$ of spline functions of order m with knots sequence $t = \{0 = t_0 < t_1 < \dots < t_{K_0} < t_{K_0+1} = 1\}$. Functions in this space have the

representation $\sum_k a_k N_{k,t}^{[m]}(x)$, where

$$N_{k,t}^{[m]}(x) = (t_k - t_{k-m})[t_{k-m}, \dots, t_k](\cdot - x)_+^{m-1}, \quad 1 \leq k \leq K = K_0 + m$$

is the k^{th} B-spline function. The notation $[t_{k-m}, \dots, t_k](\cdot - x)_+^{m-1}$ represents the m^{th} divided difference of $(\cdot - x)_+^{m-1}$ at sites t_{k-m}, \dots, t_k . This divided difference is the leading coefficient of the polynomial g of order $m+1$ that agrees with $(\cdot - x)_+^{m-1}$ at the sequence t_{k-m}, \dots, t_k . Thus if the sequence t_{k-m}, \dots, t_k is non-distinct, say with n_{t^*} values coinciding at t^* , then for $g(t)$ such that

$$(t^* - x)_+^{m-1, (i-1)} = g^{(i-1)}(t^*) \quad \text{for } i = 1, \dots, n_{t^*}$$

$[t_{k-m}, \dots, t_k](\cdot - x)_+^{m-1}$ is the coefficient of the term t^m in g . From here on, where they are obvious, we will suppress t and $[m]$ from the notation $N_{k,t}^{[m]}$.

Depending on the number of basis functions or, equivalently, the number of knots, \hat{f} can either underfit or overfit the data. Solving for the optimal number (and locations) of knots can prove very challenging (Eilers and Marx, 1996). An alternative approach is to use a large number of internal knots K_0 and regularize \hat{f} by placing a penalty on its higher-order derivatives (see, e.g., O'Sullivan, 1986; Xiao, 2019; Ramsay and Silverman, 2007); that is, to minimize

$$\sum_{i=1}^n \left\{ y_i - \sum_{k=1}^K a_k N_k(x_i) \right\}^2 + \lambda \int_0^1 \left\{ \sum_{k=1}^K a_k N_k^{(q)}(x) \right\}^2 dx \quad (4)$$

where λ is a tuning parameter whose optimal value can be found using cross validation.

We now briefly describe a matrix representation of (4) introduced by Xiao (2019). Let $\mathbf{N}(x) = [N_1(x), \dots, N_K(x)]^T \in \mathbb{R}^K$ and $\mathbf{N} = [\mathbf{N}(x_1), \dots, \mathbf{N}(x_n)]^T \in \mathbb{R}^{n \times K}$. Define $\Delta_{K,1} \in \mathbb{R}^{(K-1) \times K}$ so that, for any $\boldsymbol{\theta} \in \mathbb{R}^K$, $\Delta_{K,1}\boldsymbol{\theta} = (\theta_2 - \theta_1, \dots, \theta_K - \theta_{K-1})^T$, and define recursively the q^{th} order difference operator $\Delta_{K,q} = \Delta_{K-1,q-1}\Delta_{K,1}$, for $1 < q < K$. In addition, let $W_K^{[m]} \in \mathbb{R}^{(K-1) \times (K-1)}$ be a diagonal matrix whose k^{th} diagonal entry is equal to $(m-1)(t_k - t_{k-m+1})^{-1}$. Using this notation, we have that

$$\frac{d\mathbf{N}^{[m]}(x)}{dx} = \Delta_{K,1}^T W_K^{[m]} \mathbf{N}^{[m-1]}(x).$$

For higher order derivatives, let $\tilde{\Delta}_{K,1,m} = W_K^{[m]} \Delta_{K,1} \in \mathbb{R}^{(K-1) \times K}$ and define recursively

$\tilde{\Delta}_{K,q,m} = \tilde{\Delta}_{K-1,q-1,m-1} \tilde{\Delta}_{K,1,m}$. Then we have that

$$\frac{d^q \mathbf{N}^{[m]}(x)}{dx^q} = \tilde{\Delta}_{K,q,m}^T \mathbf{N}^{[m-q]}(x) .$$

We are now in the position to rewrite (4) as

$$\min_{\mathbf{a}} \left(\frac{1}{n} \|\mathbf{y} - N\mathbf{a}\|_2^2 + \lambda \mathbf{a}^T P_q \mathbf{a} \right) \quad (5)$$

where $\mathbf{y} = [y_1, \dots, y_n]^T$, $\mathbf{a} = [a_1, \dots, a_K]^T$ and $P_q = \tilde{\Delta}_{K,q,m}^T G^{[m-q]} \tilde{\Delta}_{K,q,m}$ with

$$G^{[m-q]} = \int N^{[m-q]}(x) N^{[m-q],T}(x) dx \in \mathbb{R}^{n \times K}.$$

Equation (5) can be solved explicitly; indeed, if we set $H_n := N^T N/n + \lambda P_q$, then the solutions are

$$\begin{aligned} \hat{\mathbf{a}} &= H_n^{-1}(N^T \mathbf{y}/n) \\ \hat{f}(x) &= N^T(x) H_n^{-1}(N^T \mathbf{y}/n). \end{aligned}$$

2.2. EM algorithm for Gaussian mixtures

Let $\xi \in \Xi$ and $z \in Z$ be random variables whose joint density function is ϕ_{θ^*} , where θ^* belongs to a (non-empty) convex parameter space Ω . Suppose we can observe data $(\xi_i)_{i=1}^n$, while the $(z_i)_{i=1}^n$ are unobservable, and that $(\xi_i | z_i = j) \stackrel{iid}{\sim} G_j$ where the G_j 's are Gaussian distributions. Our goal is to estimate the unknown θ^* using Maximum Likelihood; that is, to find $\hat{\theta}$ that maximizes

$$\ell_n(\theta) = \frac{1}{n} \sum_{i=1}^n \log \left(\int_Z \phi_\theta(\xi_i, z_i) dz_i \right) .$$

In practice, the function ℓ_n is usually hard to optimize. The EM algorithm provides a way of searching for such maximum indirectly through the maximization of another function $Q_n : \Omega \times \Omega \rightarrow \mathbb{R}$ defined as

$$Q_n(\theta | \theta') = \frac{1}{n} \sum_{i=1}^n \left(\int_Z k_{\theta'}(z | \xi_i) \log \phi_\theta(\xi_i, z) dz \right)$$

where $k_{\theta'}(z | \xi)$ is the conditional density of z given ξ . Given this function and a current estimate $\theta_{n,t}$, the sample EM update is defined as

$$\theta_{n,t+1} = \theta_{n,t} + \alpha \nabla Q_n(\theta | \theta_{n,t}) \Big|_{\theta=\theta_{n,t}}, \quad t = 0, 1, \dots .$$

To study convergence of the EM to a (neighborhood of) the global optimum, Balakrishnan et al. (2017) define the population level versions ℓ of ℓ_n and Q of Q_n as

$$\begin{aligned}\ell(\theta) &= \int_{\Xi} \log \left(\int_Z \phi_{\theta}(\xi_i, z_i) dz_i \right) g_{\theta^*}(\xi) d\xi \\ Q(\theta|\theta') &= \int_{\xi} \left(\int_Z k_{\theta'}(z|\xi_i) \log \phi_{\theta}(\xi_i, z) dz \right) g_{\theta^*}(\xi) d\xi.\end{aligned}$$

Correspondingly, one has a population version of the EM update

$$\theta_{t+1} = \theta_t + \alpha \nabla Q(\theta|\theta_t) \Big|_{\theta=\theta_t}, \quad t = 0, 1, \dots.$$

Based on this, since θ^* maximizes $\ell(\theta)$, to prove that the sample EM update converges to (a neighborhood of) θ^* , one needs to prove that (i) the population EM update converges to (a neighborhood of) θ^* ; and (ii) the sample EM update tracks closely the population update (this is precisely what we do in Proposition 4.1 and Proposition 4.2 below).

3. The **smoothEM** approach

Let us consider again data as in Equations (1) and (2); that is

$$\begin{aligned}\xi_i &:= y_i - f(x_i) = \begin{cases} \mu^* + \epsilon_i, & \text{if } x_i \in \mathbb{S} \\ \epsilon_i, & \text{otherwise} \end{cases} \\ &\sim \alpha^* N(0, \sigma^{*2}) + (1 - \alpha^*) N(\mu^*, \sigma^{*2})\end{aligned}$$

where the design (the x_i 's) is taken as fixed. If we knew f , the EM algorithm could be used to search for the MLE of the mixture parameters $\theta^* = (\alpha^*, \mu^*, \sigma^{*2})$ and to estimate membership (i.e. posterior) probabilities for each point, and thus the classification vector $\mathbb{1}_{\mathbb{S}}$. In reality, we do not know f , so we use the EM with an estimate \hat{f} of f . The traditional regularized smoothing technique in (4) is ill-fitted for the above purpose. Indeed, it declares as optimal an \hat{f} that minimizes a combination of sum of squared errors and degree of roughness. The tuning parameter λ , generally chosen by cross validation, determines the balance between these two competing criteria. In the case of noisy curves with spikes as defined in Equation (1), a sufficiently large μ^* causes the sum of squared errors term to dominate the roughness criterion. This in turns causes the cross validation

procedure to be biased towards small values of λ , i.e. towards under-smoothed \hat{f} . This is the key observation that gives rise to our iterated regularized smoothing procedure, which we illustrate through two simple examples. Figure 1 plots $n = 500$ data points

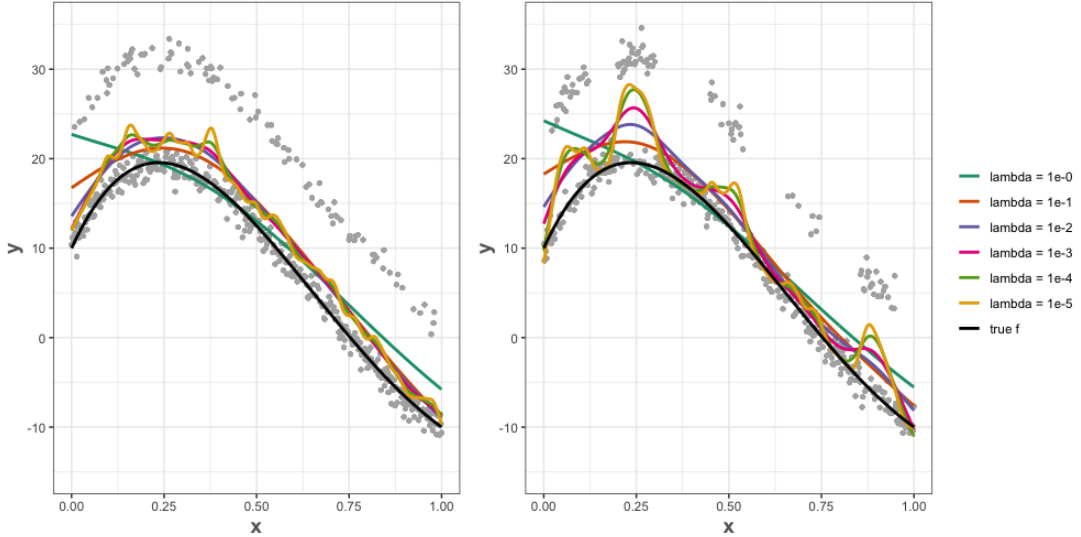


Figure 1. Simulated data and smoothing spline fit for f with different values of the tuning parameter λ (curves of different colors). Black curve represents the true f . Left: spikes are distributed independently and uniformly across the domain. Right: spikes are clustered into “hovering clouds”.

simulated across the $[0, 1]$ domain. The majority of such points are scattered about a fourth degree polynomial, the curve f , with independent errors $\epsilon_i \sim N(0, 1)$. In the left panel, spikes occur uniformly across the domain and independently from other data points, while in the right panel, spikes form “hovering clouds” of different denseness at different locations along the domain. In both scenarios, spikes are shifted vertically by $\mu^* = 12$. We note that the clustered spikes (right panel) are correlated, and thus represent a departure from our assumed mixture Gaussian model. Even if our theoretical results require independence, we show with simulations in Section 5.2 that our algorithm is robust to this departure from the theoretical assumptions, maintaining its ability to identify spikes and recover the true f also in this case. The true f is plotted in black, and the estimates \hat{f} , obtained through 300 cubic spline basis functions with equally spaced

knots and penalty of order 1, are plotted in different colors depending on the values of λ . At first glance, none of the \hat{f} 's approximates f well, though some give better fits than others. In particular, note that the presence of spikes, especially when coupled with larger λ , affects estimation at both spike and non-spike locations. Also, for the correlated case (right panel), “denser” spikes sites distort \hat{f} to a higher degree – especially for small λ values. Generalized cross-validation here selects $\lambda = 10^{-4}$, which still results in a highly distorted \hat{f} . Suppose now we were to identify spikes and do inference on the parameters $\alpha^*, \mu^*, \sigma^{*2}$ through the residuals from \hat{f} . Such a distorted estimate would generate misleading residuals. On the other hand, just from visual inspection, $\lambda = 10^{-1}$ and $\lambda = 10^{-2}$ produce much more reasonable \hat{f} 's and, correspondingly, residuals which are a much better approximation of the underlying ξ_i 's, giving some hope that one may be able to identify spikes based on their magnitudes. If we identify and filter out the spikes, and then repeat regularized smoothing, we can obtain a much improved fit to f .

3.1. *smoothEM: the algorithm*

Based on the above reasoning, we propose our ***smoothEM*** procedure, which comprises the following steps:

S1 Fit a regularized smoothing spline over a grid of λ values, and obtain the residuals

$$\boldsymbol{\xi}(\lambda) = \{\xi(\lambda)_i\}_{i=1}^n.$$

S2 For each pair $(\lambda, \boldsymbol{\xi}(\lambda))$, classify $\boldsymbol{\xi}(\lambda)$ into two groups based on their magnitudes. Label as “spikes” the group with higher magnitudes, provided its cardinality does not exceed a reasonable percentage of the total number n of observations. If no group of large residuals can be identified, or if one can be identified but it contains too many observations, then label all observations as “smooth” (none as “spikes”). The output of this step are binary group memberships $\mathbf{M}(\lambda) = \{M_i(\lambda)\}_{i=1}^n$ for each value of λ ($M_i(\lambda) = 0, 1$ means the observation (x_i, y_i) is classified as “smooth” or “spike”, respectively, when using λ in Step 1).

S3 For each pair $(\lambda, \mathbf{M}(\lambda))$, fit a second regularized smoothing spline using only observations with $M_i(\lambda) = 0$, and compute updated residuals $\boldsymbol{\xi}'(\lambda)$ for all observations.

Here we also record an “overfit” score $F(\lambda)$. The score is calculated based on how much the fit \hat{f} would change when the smooth observations ($M_i = 0$) are perturbed by a small amount.

S4 For each λ , assume that $\xi'(\lambda)$ are distributed as in Equation (2) and run the EM algorithm on $\xi'(\lambda)$, using $\mathbf{M}(\lambda)$ as initialization. This results in estimates $(\hat{\alpha}, \hat{\mu}, \hat{\sigma}^2)_\lambda$ and classification $\mathbf{M}'(\lambda)$, obtained by thresholding the EM posterior probabilities.

S5 Choose as best the λ^* that maximizes a criterion combining log-likelihood and “overfit” scores; $\lambda^* = \arg \max_\lambda [\ell(\lambda; \hat{\alpha}, \hat{\mu}, \hat{\sigma}^2) + F(\lambda)]$. Obtain estimates $(\hat{\alpha}, \hat{\mu}, \hat{\sigma}^2)_{\lambda^*}$ and update the binary memberships to $\mathbf{M}'(\lambda^*)$.

S6 Refit a regularized smoothing spline as in expression (4) with $\lambda = \lambda^*$, using only observations that satisfy $M'_i(\lambda^*) = 0$.

3.2. Some observations and remarks

An important observation is that the performance of the procedure depends critically on the grid of λ values chosen for its implementation. We can choose a relatively small grid based on prior knowledge about the smoothness of f and/or visual inspection. If there is no prior knowledge and/or visual inspection is not particularly informative, we must choose a sufficiently large and dense grid that will likely include a good λ . However, this requires fitting more smoothing splines and running more EM algorithms, at greater computational cost.

In Step 2, the initial magnitude-based classification can be done in various ways, e.g., running a 1-dimensional K -means algorithm, or based on the largest sequential difference of ordered residuals. The reasonable percentage mentioned in the same step can be determined from prior knowledge, or defaulted to be 50%.

In our experience, the overfit score F in Step 3 is especially helpful when there is a limited number of available observations, which renders the discovery of the underlying smooth structure more prone to error. Without it, sometimes the algorithm favors very small values of λ and overfits most/all of the observations, leading to near zero

residuals (almost) everywhere and producing very high likelihood values in later steps. More specifically, the overfit score F is calculated as follow. Let ξ be a collection of residuals as in Step 3 and $\xi^{(0)}$ the sub-collection corresponding to observations classified as “smooth” (i.e. with $M_i = 0$). Let $\xi_p^{(0)}$ be a perturbed version of $\xi^{(0)}$ obtained as $\xi_p^{(0)} = \xi^{(0)} + \tau$, where τ is a vector of independent variables from a $N(0, \sigma_\tau^2)$. Let $\hat{f}(\xi^{(0)})$ and $\hat{f}(\xi_p^{(0)})$ be the curves fitted to $\xi^{(0)}$ and $\xi_p^{(0)}$, respectively, and compute the score as $F = \|\hat{f}(\xi^{(0)}) - \hat{f}(\xi_p^{(0)})\|_2$. Here, the amount of perturbation can be chosen to match the overall level of noise in the original data. We recommend using a robust estimation of standard deviation, e.g., $\sigma_\tau = \text{median}(|y_i - \text{median}(\mathbf{y})|)$. We also note that the objective function in Step 5 can be generalized to $\ell(\lambda; \hat{\alpha}, \hat{\mu}, \hat{\sigma}^2) + \beta F(\lambda)$, where β can be tuned based on prior knowledge on the degree of smoothness of f .

Finally, we observe that the choice of the threshold in Step 4 also requires user input. A straightforward approach would be to classify a data point as spike if its probability of belonging to the spike group exceeds 0.5. Our implementation automatically chooses from threshold values ranging between 0.5 and 1 such that the resulting classification maximizes the log-likelihood.

4. Theoretical remarks and guarantees

4.1. Results for iterated smoothing

Here we discuss in more detail the interplay between the smoothness of f , λ , $\frac{\mu^*}{\sigma^*}$, n , and the denseness of spikes, in determining the effectiveness of iterated smoothing.

We suppose $(x_i, y_i)_{i=1}^n$ are generated as at the beginning of Section 3, but the remarks in this subsection also extend to the case of correlated spikes. For a given realization of $\mathbb{1}(x_i \in \mathbb{S})$ (i.e. with the spikes location fixed), the only randomness is from the noise $(\epsilon_i)_{i=1}^n$. Assuming without loss of generality that $\mu^* > 0$, let $r(x_p)$ and $r(x_s)$ be residuals from Step 1 at spike location x_p and smooth location x_s . The difference

$$\begin{aligned} r(x_p) - r(x_s) &= y_p - \hat{f}(x_p) - (y_s - \hat{f}(x_s)) \\ &= f(x_p) + \mu^* + \epsilon_p - N(x_p)H_n^{-1}N^T(f(\mathbf{x}) + \mu^* \cdot \mathbb{1}_{\mathbb{S}} + \boldsymbol{\epsilon})/n \\ &\quad - [f(x_s) + \epsilon_s - N(x_s)H_n^{-1}N^T(f(\mathbf{x}) + \mu^* \cdot \mathbb{1}_{\mathbb{S}} + \boldsymbol{\epsilon})/n] \end{aligned}$$

(see Section 2.1) can be decomposed as $r(x_p) - r(x_s) = R_1 + R_2 + R_3$, where

$$\begin{aligned} R_1 &= f(x_p) - N(x_p)H_n^{-1}N^T(f(\mathbf{x}) + \boldsymbol{\epsilon})/n \\ &\quad - [f(x_s) - N(x_s)H_n^{-1}N^T(f(\mathbf{x}) + \boldsymbol{\epsilon})/n] , \\ R_2 &= \mu^* - N(x_p)H_n^{-1}N^T\mu^* \cdot \mathbb{1}_S/n \\ &\quad - [0 - N(x_s)H_n^{-1}N^T\mu^* \cdot \mathbb{1}_S/n] , \\ R_3 &= \epsilon_p - \epsilon_s . \end{aligned}$$

The first component is $R_1 = r'(x_p) - r'(x_s)$, the difference of the residuals from fitting a spline to the noisy curve only. As long as the underlying true $f(x)$ is $\in C^p[0, 1]$ for $p \leq m$, where m is the order of the smoothing spline, existing literature (Xiao, 2019) guarantees that under appropriate conditions $\max_x r'(x)$ is of order $o\left\{\left(\frac{\log n}{n}\right)^{\frac{-m}{2m+1}}\right\}$. The second component is $R_2 = r''(x_p) - r''(x_s)$, the difference of the residuals from fitting a spline to the n -discretized piecewise constant $\mu^* \cdot \mathbb{1}_S$. As spline smoothing is highly localized by nature, intuitively, if the number of spikes in a neighborhood of x_p is sufficiently small and λ is sufficiently large, the smoothing spline will prioritize approximation of the constant line $g(\cdot) = 0$, causing $r''(x_p) - r''(x_s)$ to be near μ^* . As more spikes gather around x_p , this magnitude decreases, making spikes less distinguishable. It is important to note that the same λ is used to fit the noisy curve in R_1 and $\mu^* \cdot \mathbb{1}_S$ in R_2 . As a consequence, if $f(x)$ is rather jagged and thus the optimal λ to fit it is small, one may easily overfit $\mu^* \cdot \mathbb{1}_S$ – especially when spikes are dense in a neighborhood of x_p . The third component is simply $R_3 = \epsilon_p - \epsilon_s$. Under ideal conditions, R_1 will be close to 0, R_2 will be close to μ^* , and as long as $\frac{\mu^*}{\sigma^2}$ is large, the effect of R_3 will be negligible.

4.2. Results for EM

In the following, let $q(\theta) = Q(\theta|\theta^*)$ (see Section 2.2) and let $\mathbb{B}_2(r; \theta^*)$ denote an L_2 ball centered at θ^* with radius r . We start by stating three conditions that are needed to guarantee good properties for the EM algorithm:

C1 (ν -strong concavity) There is some $\nu > 0$ such that

$$q(\theta_1) - q(\theta_2) - \langle \nabla q(\theta_2), \theta_1 - \theta_2 \rangle \leq -\frac{\nu}{2} \|\theta_1 - \theta_2\|_2^2 \quad \forall \theta_1, \theta_2 \in \mathbb{B}_2(r; \theta^*);$$

C2 (Lipschitz-smoothness) There is some $L > 0$ such that

$$q(\theta_1) - q(\theta_2) - \langle \nabla q(\theta_2), \theta_1 - \theta_2 \rangle \geq -\frac{L}{2} \|\theta_1 - \theta_2\|_2^2 \quad \forall \theta_1, \theta_2 \in \mathbb{B}_2(r; \theta^*);$$

C3 (Gradient smoothness) For an appropriately small $\gamma > 0$,

$$\|\nabla q(\theta) - \nabla Q(\theta|\theta)\|_2 \leq \gamma \|\theta - \theta^*\|_2 \quad \forall \theta \in \mathbb{B}_2(r; \theta^*).$$

The Theorem below, proved in Balakrishnan et al. (2017), utilizes these assumptions to formulate guarantees for the population level EM.

THEOREM 4.1 (Balakrishnan, Wainwright & Yu, 2017). *For some radius $r > 0$ and a triplet (γ, ν, L) such that $0 \leq \gamma < \nu \leq L$, suppose that the conditions C1, C2, and C3 hold, and suppose that the stepsize is chosen as $s = \frac{2}{L+\nu}$. Then given any initialization $\theta_0 \in \mathbb{B}_2(r; \theta^*)$, with probability $1 - \delta$ the population first order EM iterates satisfy the bound*

$$\|\theta_k - \theta^*\|_2 \leq \left(1 - \frac{2\nu - \gamma}{L + \nu}\right)^k \|\theta_0 - \theta^*\|_2 \quad \text{for all } k = 1, 2, \dots$$

In the same paper, under Corollary 1, Balakrishnan et al. (2017) proves that the mixture Gaussian model meets the assumptions of the above theorem, for unknown μ^* and fixed σ^* and $\alpha^* = 0.5$. When all parameters are assumed unknown, proving the same result becomes non-trivial. The following Proposition ensures that Theorem 4.1 can be utilized in the context of our mixture Gaussian model when all parameters are assumed to be unknown (a proof is provided in the Supplementary Material).

PROPOSITION 4.1 (Population level guarantees for the Gaussian mixture). *Let ω and ω_0 denote arbitrarily small, positive numbers. Provided $\alpha^* \in [0.7, 1]$, the Gaussian mixture model in Equation (2) satisfies the conditions C1, C2 and C3 with*

- $\nu = \min \left\{ \left(\frac{1}{(\alpha^* + r)^2} \vee 1 \right), \frac{\sigma^{*2} - r}{2(\sigma^{*2} + r)^3} - \frac{(1 - \alpha^*)r}{(\sigma^{*2} - r)^2}, \frac{1 - \alpha^*}{\sigma^{*2} + r} - \frac{(1 - \alpha^*)r}{(\sigma^{*2} - r)^2} \right\}$;
- $L = \max \left\{ \frac{\alpha^*}{(\alpha^* - r \vee 0.7)^2} + \frac{1 - \alpha^*}{(1 - \alpha^* - r \vee \omega)^2}, \frac{(1 - \alpha^*)\sigma^{*2}}{(\sigma^{*2} - r)^2}, \frac{\sigma^{*2} + r}{2(\sigma^{*2} - r)^3} + \frac{1 - \alpha^*}{\sigma^{*2} - r} \right\}$;
- $\gamma(\alpha^*, \mu^*, \sigma^{*2}) \sim O \left(\frac{\mu^{*5}}{\sigma^{*8}} \exp \left(-\frac{\mu^* - r}{\sigma^{*2} + r} \omega_0 \right) \right)$, which goes to 0 exponentially fast with large $\frac{\mu^*}{\sigma^{*2}}$.

Table 1. Convergence rate $CR = \left(1 - \frac{2\nu - \gamma}{L + \nu}\right)$ and number of iterations k that guarantees $CR^k < 0.0001$, for different values of σ^* , α^* and r .

$(CR; k)$	(σ^*, r)				
	(1.1,0.37)	(2.1,0.7)	(3.1,1.03)	(4.1,1.37)	(5.1,1.7)
.1	(0.984,40)	(0.795,17)	(0.807,17)	(0.852,23)	(0.894,32)
.05	(0.991,70)	(0.795,17)	(0.667,10)	(0.702,15)	(0.752,18)

Before proceeding, some remarks are in order on the use of Proposition 4.1. First, ν decreases as r increases; this creates an undesirable trade off, as ideally we would want both to be large. A larger r allows for a larger basin of attraction for convergence, whereas a larger ν hastens the convergence rate. Identifying a large r for which $\nu > 0$ requires solving a $^{\text{th}}$ degree polynomial. As a bypass, Table 1 provides some admissible $(r; \nu)$ pairs for various parameter settings. It is reasonable to anchor r to the error variance σ^{*2} ; for instance, taking $r = \frac{\sigma^*}{3}$ leads to a positive value of ν in most cases.

Second, even with a positive ν , the convergence rate can be slowed by a large Lipschitz smoothness constant L in the assumption C2. In particular, an arbitrarily large $\frac{1-\alpha^*}{(1-\alpha^*-r \vee \omega)^2}$ makes the rate $\left(1 - \frac{2\nu - \gamma}{L + \nu}\right)^k$ unacceptably slow. Interestingly, a way to upper-bound L is to upper-bound α^* (i.e. to require that spikes are present in a non-negligible amount); for instance, setting $\alpha^* \leq 0.95$. This affords small gains though; even under ideal circumstances, we only manage to get the convergence rate down to 0.999^k , which is still very slow.

There might be other approaches to guarantee fast convergence in a problem like ours where, in addition to μ^* , α^* and σ^{*2} are unknown. While we are unaware of such approaches, we are reassured by the fact that our simulations provide evidence of reasonable convergence rates with our procedure (see Section 5).

We conclude by noting that if, like the majority of current literature, we assumed known α^* and σ^{*2} , there would be no convergence issues. In this case $\nu = L$, and it is straightforward to prove that population updates converge geometrically to the true population parameters provided that the ratio $\frac{\mu^*}{\sigma^{*2}}$ is large enough. Notably, if we assume only that α^* is known (so both μ^* and σ^{*2} are unknown) we can still obtain a reason-

able convergence rate using $r = \frac{\sigma^*}{3}$, $\nu = \min \left\{ \frac{\sigma^{*2}-r}{2(\sigma^{*2}+r)^3} - \frac{(1-\alpha^*)r}{(\sigma^{*2}-r)^2}, \frac{1-\alpha^*}{\sigma^{*2}+r} - \frac{(1-\alpha^*)r}{(\sigma^{*2}-r)^2} \right\}$, $L = \max \left\{ \frac{(1-\alpha^*)\sigma^{*2}}{(\sigma^{*2}-r)^2}, \frac{\sigma^{*2}+r}{2(\sigma^{*2}-r)^3} + \frac{1-\alpha^*}{\sigma^{*2}-r} \right\}$ and $\gamma(\alpha^*, \mu^*, \sigma^{*2}) \sim O \left(\frac{\mu^{*5}}{\sigma^{*8}} \exp(-\frac{\mu^*-r}{\sigma^{*2}+r} \omega_0) \right)$.

Next, we consider a Theorem for the sample EM, also proved in Balakrishnan et al. (2017).

THEOREM 4.2 (Balakrishnan, Wainwright & Yu, 2017). *For a given size n and tolerance parameter $\delta \in (0, 1)$, let $\epsilon_Q^{unif}(n, \delta)$ be the smallest scalar such that with probability at least $1 - \delta$*

$$\sup_{\theta \in \mathbb{B}_2(r; \theta^*)} \|\nabla Q_n(\theta | \theta) - \nabla Q(\theta | \theta)\|_2 \leq \epsilon_Q^{unif}(n, \delta) .$$

Suppose that, in addition to the conditions of Theorem (4.1), the sample size n is large enough to ensure that

$$\epsilon_Q^{unif}(n, \delta) \leq (\nu - \gamma)r .$$

Then with probability at least $1 - \delta$, given any initial vector $\theta_0 \in \mathbb{B}_2(r; \theta^)$, the finite sample EM iterates $\{\theta_k\}_{k=0}^{\infty}$ satisfy the bound*

$$\|\theta_t - \theta^*\|_2 \leq \left(1 - \frac{2\nu - 2\gamma}{L + \nu} \right)^t \|\theta_0 - \theta^*\|_2 + \frac{\epsilon_Q^{unif}(n, \delta)}{\nu - \gamma} .$$

Based on this Theorem, we have the following Proposition concerning our problem (a proof is provided in the Supplementary Material).

PROPOSITION 4.2 (Sample level guarantees for the Gaussian mixture). *For the Gaussian mixture model in Equation (2), $\epsilon_Q^{unif}(n, \delta) \rightarrow 0$ almost surely.*

Combined with Proposition 4.1, Proposition 4.2 means that sample EM updates have the same convergence rate as the population updates, asymptotically.

5. Simulation results

In the following simulations, $(x_i)_{i=1}^n$ are equispaced along the interval $[0, 1]$. The true smooth component is a polynomial of degree 4 (or, equivalently, of order 5). Due to the local nature of spline basis, different distributions of spike locations affect traditional

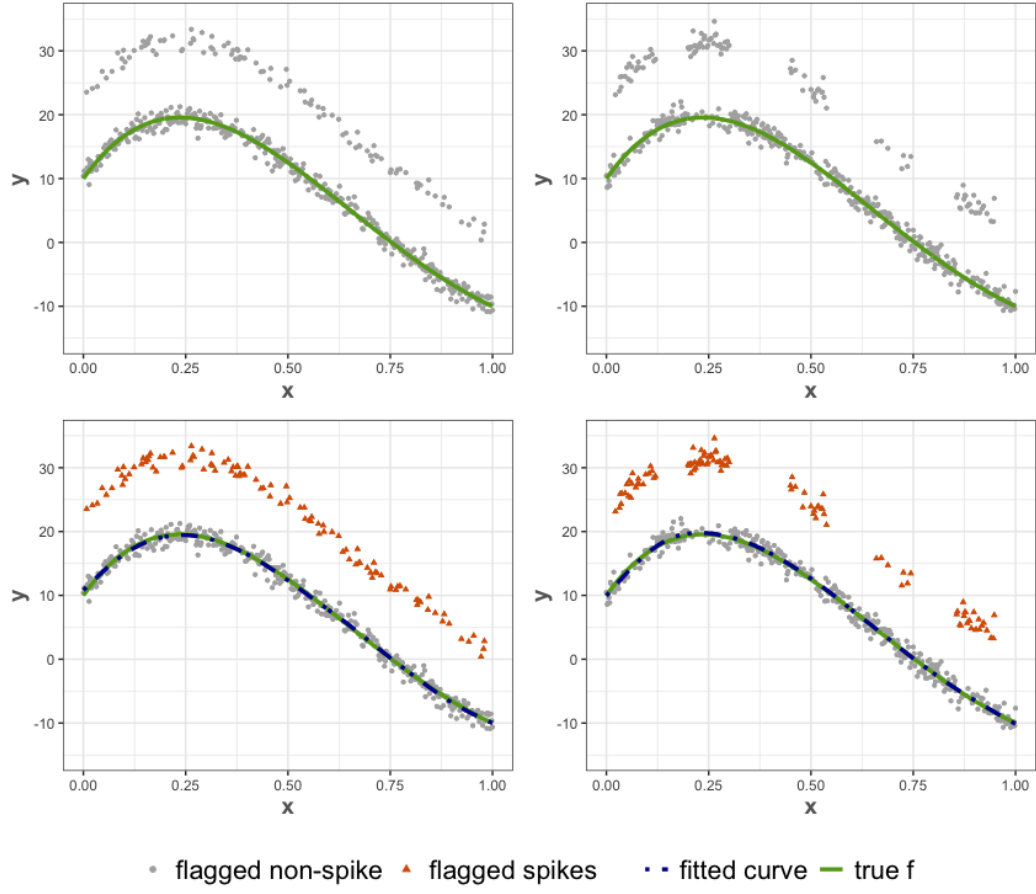


Figure 2. Top: Simulated data with uniformly distributed spikes (left) and clustered spikes (right). In both cases: $n = 500$, $\sigma^* = 1$, $\alpha^* = 0.80$, $\mu^* = 12$. Bottom: corresponding results from fitting the smooth curve and identifying the spikes. The true smooth curve and the fitted curve are plotted in green solid line and blue dotted line, respectively; flagged spikes and non-spikes are plotted in red triangles and gray circles, respectively.

spline smoothing methods differently. Therefore, as in the examples of Figure 1, we consider two different simulation scenarios: one in which spikes are uniformly distributed across the domain, and one in which they are “clumped”. The two top panels of Figure 2 show these two scenarios (the green curves represent the true smooth component f). The bottom panels of Figure 2 show the results from fitting the smooth curve and

identifying the spikes with *smoothEM*. The fitted curve \hat{f} is shown as a blue dotted line, and points flagged as spikes are plotted as red triangles. In both scenarios, the fitted curve \hat{f} matches the true smooth curve f very closely. The improvement over the example of Figure 1, where the fitted curves are obtained using traditional smoothing splines, is obvious.

In the following subsections, we demonstrate in detail the performance of *smoothEM* in the two scenarios, for several different settings. More specifically, we look at how the proposed procedure performs for $n = 2000, 1000, 500, 200$, α^* ranging from 0.8 to 0.98 (i.e. for spike contamination levels between 0.2 and 0.02), and “signal to noise” (SNT) ratios $\frac{\mu^*}{6\sigma^*}$ ranging from 0.2 to 2 – these are implemented fixing $\sigma^* = 1$ and changing the spike size parameter μ^* . Note that the factor $6\sigma^*$ represents the width of the 95% Gaussian noise interval at any given location. Thus, for instance, if (x_i, y_i) lies $3\sigma^*$ below $f(x_i)$, and if $x_i \in \mathbb{S}$, then $\mu^* = 2 \cdot 6\sigma^*$ brings (x_i, y_i) to a height well separated from the smooth underlying pattern, $3\sigma^*$ above the graph of f .

5.1. Uniformly distributed spikes

Figure 3 contains contour plots of $\|\hat{f} - f\|_2$ for $n = 200, 500, 1000, 2000$. Each plot shows how $\|\hat{f} - f\|_2$ varies with different spike percentages (α^*) and SNTs ($\frac{\mu^*}{6\sigma^*}$). For each parameter setting, the results shown are averages over 20 replicates of the simulation. Figure 4 contains similar plots for the False Negative Rate (FNR) in spike identification. Results for the False Positive Rate (FPR) are not shown because our procedure has excellent specificity in all parameters settings considered; the maximum FPR is 0.02.

We observe that, when n is large, a sufficiently large signal ($\frac{\mu^*}{6\sigma^*} \geq 1$) corresponds to low FNR (i.e. good classification power), and thus low error in estimating the smooth component. When the signal is small, so that spikes are not well separated, our procedure naturally has a harder time recognizing them. However, estimation of the smooth component does not suffer much in these settings, as smaller spikes do not distort the fit substantially. Notably though, both spike identification and estimation of the smooth component do improve with larger spike size and lower α^* , which is in line with our previous discussion in Section 4. Figure 5 contains contour plots of the sum of squared

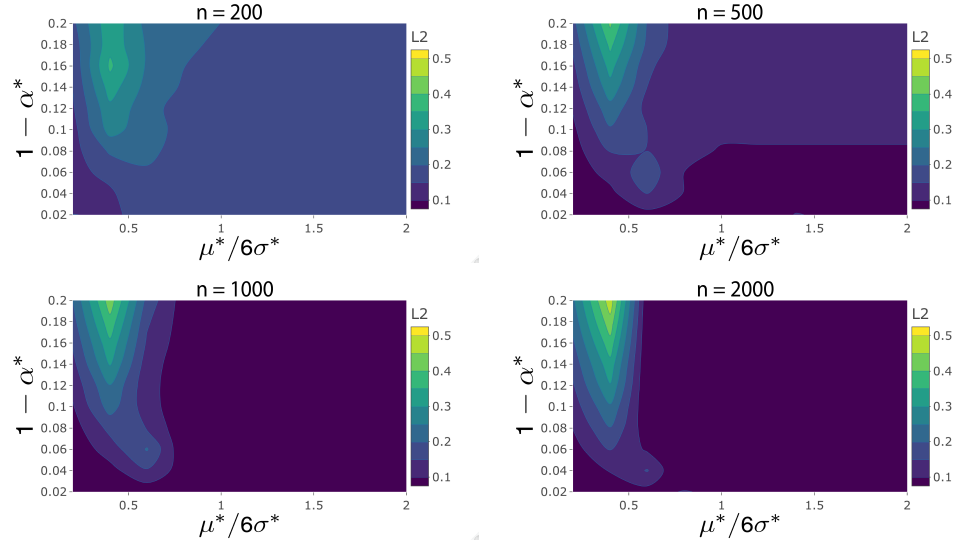


Figure 3. L_2 error of the smooth component estimate for simulated data with uniformly distributed spikes. The contour plots show the error (averaged over 20 simulation replicates) as a function of the spike percentage ($1 - \alpha^*$) and the STN ($\frac{\mu^*}{6\sigma^*}$). From left to right, top to bottom, $n = 200$, $n = 500$, $n = 1000$, $n = 2000$.

error of parameter estimates $\|\hat{\theta} - \theta^*\|_2$, with the same format as Figures 3 and 4. Here the accuracy of parameter estimation is consistent with FNR results, which is to be expected since the misclassification of spikes affects estimation of μ^*, σ^* and α^* .

5.2. Non-homogeneous Poisson spikes

The top-right panel in Figure 2 depicts a scenario where spike locations are generated through a non-homogeneous Poisson, as to be “clumped” – instead of uniformly distributed across the domain. To achieve this, our simulation uses a thinning method by Lewis and Shedler (1979). Following their algorithm, the rate function is chosen such that we have spike “clumps” of difference sizes. We note that by using a non-homogeneous Poisson distribution, at best, we can only approximate the percentage of contamination. As the locations of spikes are now correlated, the mixture Gaussian model specification will not apply. However, simulation results demonstrate excellent robustness for this type of model mis-specification. Figures S1-S3 in the Supplementary

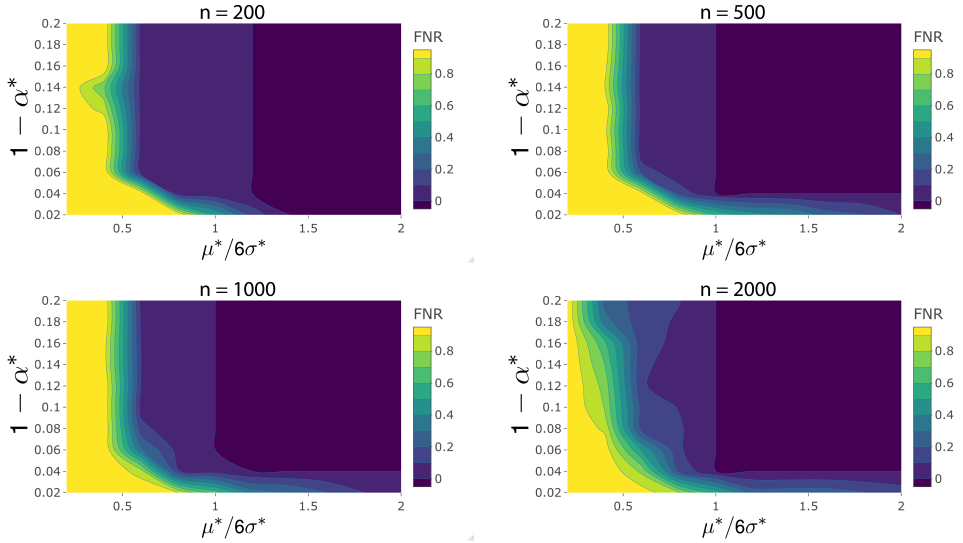


Figure 4. FNR of spike identification for simulated data with uniformly distributed spikes. The contour plots show the FNR (averaged over 20 simulation replicates) as a function of the spike percentage ($1 - \alpha^*$) and the SNT ($\frac{\mu^*}{6\sigma^*}$). From left to right, top to bottom, $n = 200$, $n = 500$, $n = 1000$, $n = 2000$.

Material are the analogs of Figures 3-5 – and they look very similar to the latter. This suggests that our procedure performs similarly well, and thus that it possesses a degree of robustness to the different ways spikes may be distributed across the domain.

6. Data applications

6.1. Extreme temperatures in US

For our first application, we consider two temperature-related time series in the US, covering the period from 1910 to 2015. The first is the series of the annual heatwave index. This index treats as a heatwave any period of four or more days with an unusually high average temperature (i.e. an average temperature that is expected to occur once every 10 years), and takes on values as a function of geographical spread and frequency of heatwaves. The second is the series of the annual percentage of US land area with unusually high summer temperatures. A visual inspection of the two time series, shown in Figure 6, suggests that assuming the error variances at smooth and spike locations to

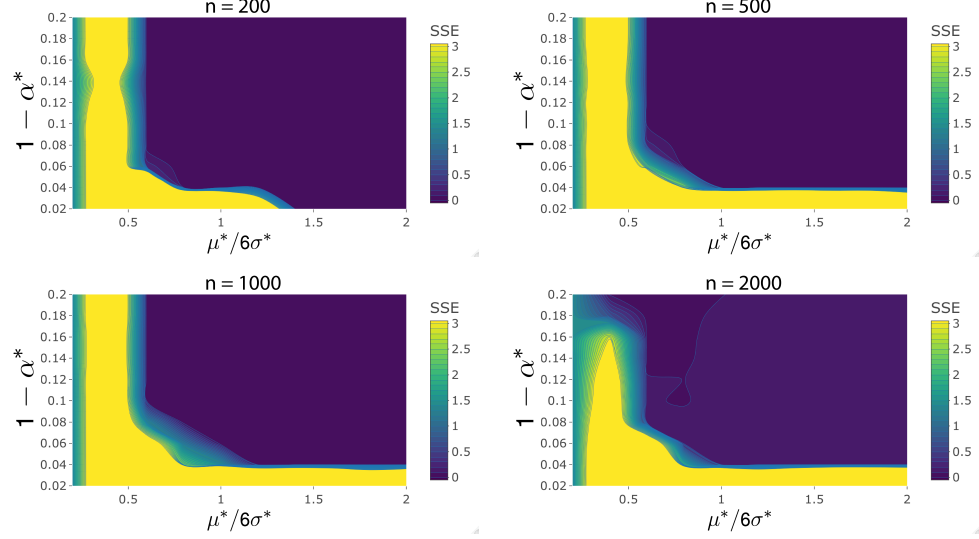


Figure 5. SSE of parameter estimates for simulated data with uniformly distributed spikes. The contour plots show the SSE (averaged over 20 simulation replicates) as a function of the spike percentage (α^*) and the SNT ($\frac{\mu^*}{6\sigma^*}$). From left to right, top to bottom, $n = 200$, $n = 500$, $n = 1000$, $n = 2000$.

be the same, as we do in Equation (2), may be too restrictive here. Because of this, we allow errors to have not only a mean shift but also inflated variance at spike locations; that is, we use the model

$$\xi_i \sim \alpha^* N(0, \sigma_\epsilon^{*2}) + (1 - \alpha^*) N(\mu^*, \sigma_\epsilon^{*2} + \sigma_h^{*2}) . \quad (6)$$

This adds a new variance parameter to be estimated in the EM algorithm, which is not covered in our theoretical treatment in Section 4.2, but does not cause any convergence slow-down in this application. Using the grid (1000,100,10,1,0.1,0.01,0.001,0.0001) for the tuning parameter λ , our procedure yields the spike identification and estimated smooth curves shown in red triangles and green lines, respectively, in Figure 6. Probably because geographical spread is part of the definition of the heatwave index, the two time series show rather similar underlying trends. Our procedure is able to detect the 1936 North American heat wave, one of the most intense in modern history, both in terms of heat index and of US area affected by high temperatures – along with a number of

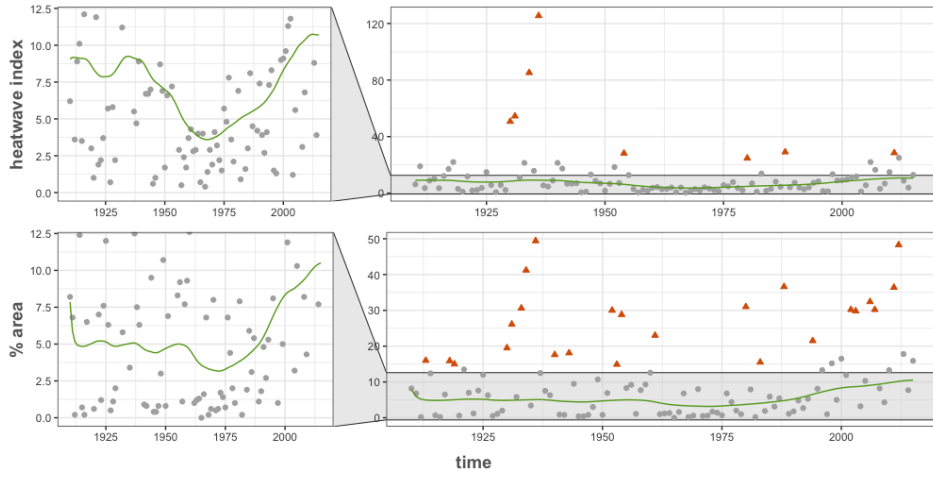


Figure 6. Annual heatwave index in the United States (top) and share of US land with unusually high summer temperature (bottom). The estimated smooth component is plotted in green, whereas spikes are identified by the red triangles. For each plot, a vertical zoom (on the left) allows us to visualize the upward trend in the smooth components of both signals in recent decades.

other spikes. Interestingly, only one spike detected in the heatwave index series concerns recent decades – likely due to the fact that the smooth component estimate exhibits an upward trend; what classified as a spike in the 50’s, or even the 80’s, is consistent with a standard oscillation around a growing systematic value in more recent times. The picture is different for the US area time series; here recent decades exhibit both an increasing smooth component estimate and an abundance of detected spikes – suggesting that the geographical dimension of the problem may be yet more concerning. The estimated values for α^* , μ^* , σ_ϵ^{*2} , σ_h^{*2} are respectively 0.08, 30.83, 5.77, 30.79 for the heatwave index, and 0.28, 17.88, 3.96, 10.49 for the US area.

6.2. Smart meter electricity data

In our second application, we consider data from the Smart Meter Electricity project of the Irish Commission for Energy Regulation (CER), which collected data on electricity consumption from over 5000 households and businesses during 2009 and 2010. Our goal

here is to create a meaningful statistical representation of the electricity consumption behavior, which may be useful to policy makers. We assume that consumption predom-

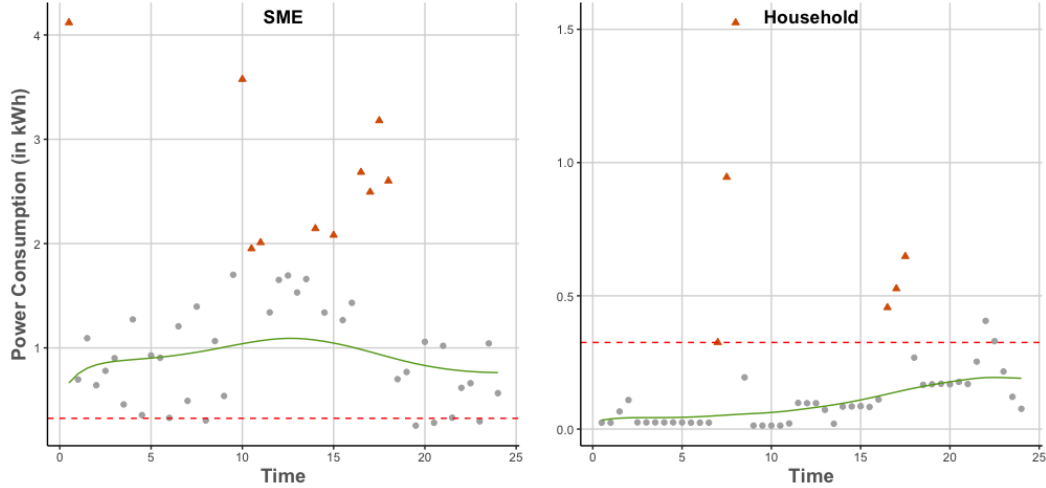


Figure 7. Electricity consumption by an Irish small business (left) and an Irish household (right) on Jan 5, 2010. The estimated smooth components are plotted in green, whereas spikes are identified by red triangles. The red horizontal dashed lines placed at 0.3 on the vertical axes help visualize the different magnitudes of consumption for the two types of users.

inantly follows a smooth pattern with occasional spiked activity – for example during the times when multiple electrical devices are turned on simultaneously – and we model the data within our framework. The data contains daily measurements of electricity consumed, collected at 30 minute intervals in kWh, for each household and business in the study. As an illustration, we run our procedure on data from one household (meter ID 1976) and one small business enterprise (SME, meter ID 1977) for the months of January and July in 2010. This allows us to highlight differences in patterns of power usage between households and business, and winter and summer months. Also for this data, visual inspection suggests that errors at spike locations have both a mean shift and an inflated variance. This can be appreciated in Figure 7, which refers to January 5, 2010. We thus use again the model in Equation (6). We also adopt again the grid $(1000, 100, 10, 1, 0.1, 0.01, 0.001, 0.0001)$ for the tuning parameter λ . The spike identifica-

tion and estimated smooth curves generated by our procedure for January 5, 2010, are shown in red triangles and green lines, respectively, in Figure 7. Figure 8 shows esti-

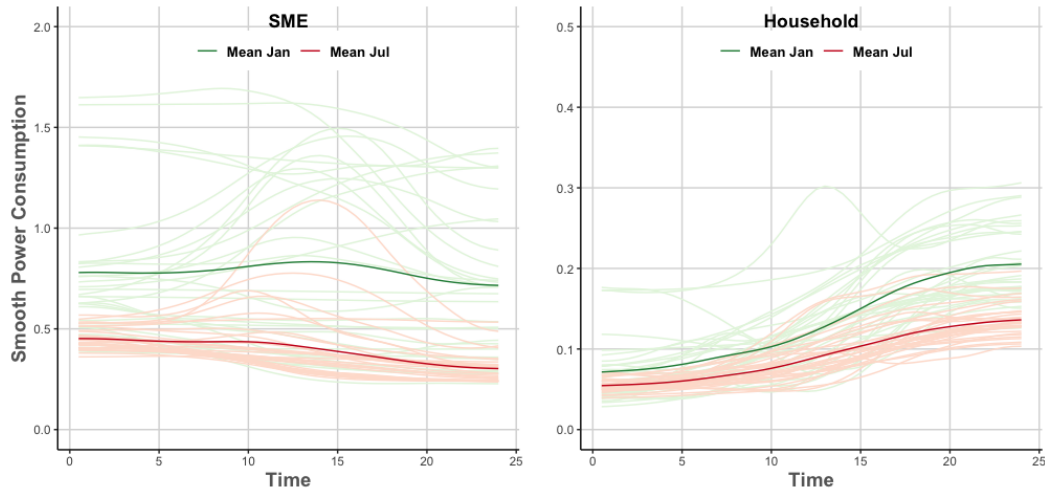


Figure 8. Electricity consumption by an Irish small business (left) and an Irish household (right) for the months of January and July, 2010. Estimated smooth components for each day in January and July are plotted in light green and light red, respectively. The corresponding monthly means are plotted in darker green/red.

mated smooth curves for the household and small business considered across all January and July days. We clearly see that, for both entities, power consumption is higher in January (likely due to heating during cold weather) but follows the same daily pattern in January and July. We also clearly see that such daily pattern is rather different for the small business and the household. Power usage tends to peak during the day for the former and at night for the latter. Notably, power usage by the small business is also more variable (from one day to another) than that by the household – which appears much more consistent. Figure 9 shows monthly frequencies of estimated spikes in every hour of the day, plotted again for the household and small business considered and for January and July. Notably, the household spikes predominantly occur in the early morning (7:00-8:00am) and, in January, in mid-afternoon (4:00-5:00pm). The small business has numerous spikes in the period of the day when its smooth consumption component

is highest (approximately 10:00am to 5:00pm) and, interestingly, right after midnight – this may correspond to the automatic activation of some appliances.

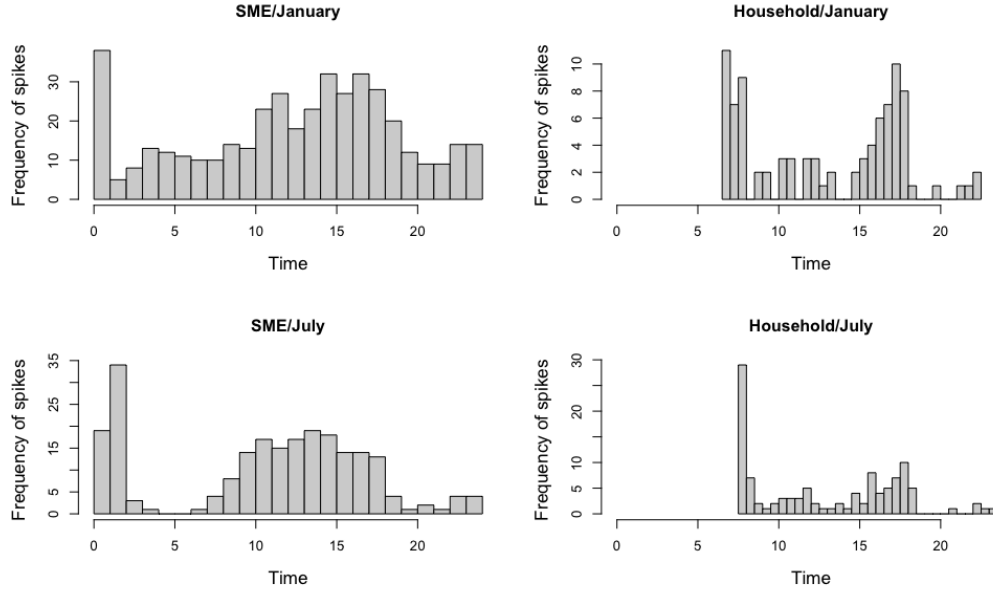


Figure 9. Electricity consumption by an Irish small business (left) and an Irish household (right) for the months of January and July, 2010. Frequencies of estimated spikes for each hour of the day during January (top) and July (bottom).

7. Discussion

In this article we propose a procedure that, given a signal, simultaneously performs estimation of its smooth component and identification of spikes that may be interspersed within it. Our procedure uses regularized spline smoothing techniques and the EM algorithm, and is suited to analyze data with discontinuous irregularities superimposed to a noisy curve. This type of data occurs in many applications. We lay out conditions for the procedure to work, and prove asymptotic convergence properties of the EM to a neighborhood of the global optimum under certain restricted conditions. We also demonstrate the effectiveness of the procedure under departures from such restricted conditions through simulations and two real data applications.

Notably, since it separates spikes and smooth component, our procedure could also be used as a way to pre-process functional data prior to the use of other FDA tools. For instance, in a regression context, instead of introducing a functional predictor obtained through traditional spline smoothing of the raw data, one could apply our procedure and introduce two distinct predictors; namely, the estimated \hat{f} and, separately, the flagged spike locations. As another example, when performing motif discovery or local clustering for sets of curves (Cremona and Chiaromonte, 2020), our procedure could produce “de-spiked” versions of the curves to be searched for recurring smooth patterns, and patterns of detected spikes could be analyzed separately. We shall leave these and other possibilities for future work.

In addition, we note that neither in our simulation study nor in the data applications we compared our approach to other existing methods. This is because, to our knowledge, none exists that targets the same type of data structure and problem. Perhaps the closest method known to us is Descary and Panaretos (2019), in which the authors also assume an additive structure comprising smooth and “rough” components. However, their “rough” component is assumed to be smooth at finer scales. Thus, their approach does not allow for discontinuous spikes like ours does and, as a consequence, cannot tackle spike identification.

Finally, an implementation of the methodology in R and some examples are provided at <https://github.com/hqd1/smoothEM>

Acknowledgements

The extreme temperature data was obtained from the National Oceanic and Atmospheric Administration (NOAA) via the Environmental Protection Agency (APE) website. We thank the Irish Social Science Data Archive for having generously provided access to the Smart Meter Electricity data. M.A. Cremona acknowledges the support of the Natural Sciences and Engineering Research Council of Canada (NSERC) and of the Faculty of Business Administration of Université Laval. F. Chiaromonte acknowledges the support of the Huck Institutes of the Life Sciences of the Pennsylvania State University.

References

Balakrishnan, S., Wainwright, M. J. and Yu, B. (2017) Statistical guarantees for the EM algorithm: from population to sample-based analysis. *The Annals of Statistics*, **45**, 77–120.

de Boor, C. (1978) *A practical guide to splines*. Springer.

Claeskens, G., Krivobokova, T. and Opsomer, J. D. (2009) Asymptotic properties of penalized spline estimators. *Biometrika*, **96**, 529–544.

Cremona, M. A. and Chiaromonte, F. (2020) Probabilistic k-mean with local alignment for clustering and motif discovery in functional data. *arXiv*, 1808.04773.

Dempster, A. P., Laird, N. M. and Rubin, D. B. (1977) Maximum likelihood from incomplete data via the EM algorithm. *Journal of the Royal Statistical Society: Series B (Statistical Methodology)*, **39**, 1–38.

Descary, M. H. and Panaretos, V. M. (2019) Functional data analysis by matrix completion. *The Annals of Statistics*, **47**, 1–38.

Eilers, P. and Marx, B. (1996) Flexible smoothing with B-splines and penalties (with Discussion). *Statistical Science*, **11**, 89–121.

Eilers, P., Marx, B. and Durban, M. (2015) Twenty years of p-splines. *SORT*, **39**, 149–186.

Goldsmith, J., Bobb, J., Crainiceanu, C. M., Caffo, B. and Reich, D. (2011) Penalized functional regression. *Journal of Computational and Graphical Statistics*, **20**, 830–851.

Hall, P. and Opsomer, J. D. (2015) Theory for penalised spline regression. *Biometrika*, **92**, 105–118.

Kauermann, G., Krivobokova, T. and Fahrmeir, L. (2009) Some asymptotic results on generalized penalized spline smoothing. *Journal of the Royal Statistical Society: Series B (Statistical Methodology)*, **71**, 487–503.

Kokoszka, P. and Reimherr, M. (2017) *Introduction to Functional Data Analysis*. CRC Press.

Lewis, P. A. W. and Shedler, G. S. (1979) Simulation of Nonhomogeneous Poisson Processes with Degree-Two Exponential Polynomial Rate Function. *Operations Research*, **27**, 1026–1040.

Liu, C. and Rubin, D. B. (1994) The ECME algorithm: A simple extension of EM and ECM with faster monotone convergence. *Biometrika*, **81**, 633–648.

Louis, T. A. (1982) Finding the observed information matrix when using the EM algorithm. *Journal of the Royal Statistical Society: Series B (Statistical Methodology)*, **44**, 226–233.

Meilijson, I. (1989) A fast improvement to the EM algorithm on its own terms. *Journal of the Royal Statistical Society: Series B (Statistical Methodology)*, **51**, 127–138.

Meng, X. and Rubin, D. B. (1993) Maximum likelihood estimation via the ECM algorithm: A general framework. *Biometrika*, **80**, 267–278.

Nason, G. P. (2008) *Wavelet Methods in Statistics with R*. Springer.

O’Sullivan, F. (1986) A statistical perspective on ill-posed inverse problems. *Statistical Science*, **1**, 502–518.

Ramsay, J. O. and Silverman, B. (2007) *Applied functional data analysis: methods and case studies*. Springer.

Wang, X., Shen, J. and Ruppert, D. (2011) On the asymptotics of penalized spline smoothing. *Electronic Journal of Statistics*, **5**, 1–17.

Wood, S. (2006) Low-rank scale-invariant tensor product smooths for generalized additive mixed models. *Biometrics*, **62**, 1025–1036.

Wu, C., Yang, C., Zhao, H. and Zhu, J. (2017) On the convergence of the em algorithm: A data-adaptive analysis. ArXiv:1611.00519v2.

Xiao, L. (2019) Asymptotic theory of penalized splines. *Electronic Journal of Statistics*, **13**, 747–794.

Xiao, L., Li, C., Checkley, W. and Crainiceanu, C. (2018) Fast covariance estimation for sparse functional data. *Statistics and Computing*, **28**, 511–522.

Xiao, L., Zipunnikov, V., Ruppert, D. and Crainiceanu, C. (2016) Fast covariance estimation for high-dimensional functional data. *Statistics and Computing*, **26**, 409–421.

Yao, F. and Lee, T. C. M. (2006) Penalized spline models for functional principal component analysis. *Journal of the Royal Statistical Society: Series B (Statistical Methodology)*, **68**, 3–25.

smoothEM: a new approach for the simultaneous assessment of smooth patterns and spikes - supplementary material

Huy Dang

Department of Statistics, The Pennsylvania State University, University Park, USA.

E-mail: hqd1@psu.edu

Marzia A. Cremona

Department of Operations and Decision Systems, Université Laval, Québec, Canada.

CHU de Québec – Université Laval Research Center, Québec, Canada

Francesca Chiaromonte

Department of Statistics, The Pennsylvania State University, University Park, USA.

Institute of Economics and EMbeDS, Sant'Anna School of Advanced Studies, Pisa, Italy.

S1 Proofs

S1.1 Proof of Proposition 4.1

Proof. In order to prove the convergence of the EM at the population level, we need to ensure that the three conditions C1, C2 and C3 in Balakrishnan et al. (2017) are satisfied.

C1) The first condition is ν -strong concavity, i.e. there is some $\nu > 0$ such that

$$q(\theta_1) - q(\theta_2) - \langle \nabla q(\theta_2), \theta_1 - \theta_2 \rangle \leq -\frac{\nu}{2} \|\theta_1 - \theta_2\|_2^2.$$

We have

$$q(\theta) = Q(\theta|\theta^*) = \mathbb{E}_{\theta^*} \left[\frac{1}{A^* + B^*} (A^* \log A + B^* \log B) \right]$$

where $A = \alpha\phi(\xi; 0, \sigma^2)$ and $B = (1 - \alpha)\phi(\xi; \mu, \sigma^2)$.

Let $f = -q$, then the strong concavity of q is equivalent to the strong convexity of f .

Since f is twice continuously differentiable, this strong convexity condition is equivalent to the positive semidefiniteness of $\nabla^2 f(\theta) - \nu I$ for every $\theta \in \mathbb{B}_2(r; \theta^*)$, where I is the identity matrix, see proposition B.5 in Bertsekas (1995).

We have

$$\begin{aligned} \nabla f(\theta) &= \mathbb{E} \left\{ \frac{1}{A^* + B^*} \left(\frac{B^*}{1-\alpha} - \frac{A^*}{\alpha} \right), \right. \\ &\quad \frac{-B^*(\xi - \mu)}{(A^* + B^*)\sigma^2}, \\ &\quad \left. \frac{A^*}{A^* + B^*} \left(\frac{1}{2\sigma^2} - \frac{\xi^2}{2\sigma^4} \right) + \frac{B^*}{A^* + B^*} \left(\frac{1}{2\sigma^2} - \frac{(\xi - \mu)^2}{2\sigma^4} \right) \right\}. \end{aligned}$$

Differentiating one more time, we get

$$\begin{aligned} \nabla^2 f(\theta) &= \mathbb{E} \begin{bmatrix} \frac{1}{A^* + B^*} \left(\frac{B^*}{(1-\alpha)^2} + \frac{A^*}{\alpha^2} \right) & 0 & 0 \\ 0 & \frac{B^*}{(A^* + B^*)\sigma^2} & \frac{B^*}{A^* + B^*} \frac{(\xi - \mu)}{\sigma^4} \\ 0 & \frac{B^*}{A^* + B^*} \frac{(\xi - \mu)}{\sigma^4} & \frac{A^*}{A^* + B^*} \left(-\frac{1}{2\sigma^4} + \frac{\xi^2}{\sigma^6} \right) + \frac{B^*}{A^* + B^*} \left(-\frac{1}{2\sigma^4} + \frac{(\xi - \mu)^2}{\sigma^6} \right) \end{bmatrix} \\ &= \begin{bmatrix} \frac{\alpha^*}{\alpha^2} + \frac{1-\alpha^*}{(1-\alpha)^2} & 0 & 0 \\ 0 & \frac{1-\alpha^*}{\sigma^2} & \frac{(1-\alpha^*)(\mu^* - \mu)}{\sigma^4} \\ 0 & \frac{(1-\alpha^*)(\mu^* - \mu)}{\sigma^4} & \alpha^* \left(-\frac{1}{2\sigma^4} + \frac{\sigma^{*2}}{\sigma^6} \right) + (1-\alpha^*) \left(-\frac{1}{2\sigma^4} + \frac{\sigma^{*2}}{\sigma^6} \right) \end{bmatrix} \\ &= \begin{bmatrix} \frac{\alpha^*}{\alpha^2} + \frac{1-\alpha^*}{(1-\alpha)^2} & 0 & 0 \\ 0 & \frac{1-\alpha^*}{\sigma^2} & \frac{(1-\alpha^*)(\mu^* - \mu)}{\sigma^4} \\ 0 & \frac{(1-\alpha^*)(\mu^* - \mu)}{\sigma^4} & \left(-\frac{1}{2\sigma^4} + \frac{\sigma^{*2}}{\sigma^6} \right) \end{bmatrix}. \end{aligned}$$

Thus,

$$\nabla^2 f(\theta) - \nu I = \begin{bmatrix} \frac{\alpha^*}{\alpha^2} + \frac{1-\alpha^*}{(1-\alpha)^2} - \nu & 0 & 0 \\ 0 & \frac{1-\alpha^*}{\sigma^2} - \nu & \frac{(1-\alpha^*)(\mu^* - \mu)}{\sigma^4} \\ 0 & \frac{(1-\alpha^*)(\mu^* - \mu)}{\sigma^4} & \left(-\frac{1}{2\sigma^4} + \frac{\sigma^{*2}}{\sigma^6} \right) - \nu \end{bmatrix} = \begin{bmatrix} a & 0 & 0 \\ 0 & b & c \\ 0 & c & d \end{bmatrix}.$$

The task becomes finding a $\nu > 0$ such that the matrix above is positive semidefinite, or equivalently, such that all principal minors are nonnegative. This means we need to ensure:

(a) $a \geq 0$.

We note that for $\theta \in \mathbb{B}_2(r; \theta^*)$, it's true that $\alpha > 0.5$, and $\frac{\alpha^*}{\alpha^2} + \frac{1-\alpha^*}{(1-\alpha)^2} \geq \frac{\alpha^*}{\alpha^2} + \frac{1-\alpha^*}{\alpha^2} = \frac{1}{\alpha^2} > \frac{1}{(\alpha^* + r \wedge 1)^2}$. Thus this condition is satisfied for $\nu < \frac{1}{(\alpha^* + r \wedge 1)^2}$;

(b) $b \geq 0$.

This is satisfied if $\nu < \frac{1-\alpha^*}{\sigma^{*2}+r}$;

(c) $d \geq 0$.

Note that

$$\inf_{\sigma^2 \in \mathbb{B}_2(r; \sigma^{*2})} -\frac{1}{2\sigma^4} + \frac{\sigma^{*2}}{\sigma^6} = \frac{\sigma^{*2} - r}{2(\sigma^{*2} + r)^3}, \text{ if } r < \sigma^{*2}.$$

Thus, this condition is satisfied if $\nu < \frac{\sigma^{*2} - r}{2(\sigma^{*2} + r)^3}$ and $r < \sigma^{*2}$;

(d) $bd - c^2 \geq 0$.

If $\frac{1-\alpha^*}{\sigma^{*2}+r} \geq \frac{\sigma^{*2}-r}{2(\sigma^{*2}+r)^3}$, we combine with $\frac{(1-\alpha^*)(\mu^*-\mu)}{\sigma^4} \leq \frac{(1-\alpha^*)r}{(\sigma^{*2}-r)^2}$ to reduce the last condition to a stricter one of $\frac{\sigma^{*2}-r}{2(\sigma^{*2}+r)^3} - \nu \geq \frac{(1-\alpha^*)r}{(\sigma^{*2}-r)^2}$, or equivalently, $\nu \leq \frac{\sigma^{*2}-r}{2(\sigma^{*2}+r)^3} - \frac{(1-\alpha^*)r}{(\sigma^{*2}-r)^2}$. If for some values of σ^{*2} , $\frac{1-\alpha^*}{\sigma^{*2}+r} \leq \frac{\sigma^{*2}-r}{2(\sigma^{*2}+r)^3}$, then by similar reasoning, we require $\nu \leq \frac{1-\alpha^*}{\sigma^{*2}+r} - \frac{(1-\alpha^*)r}{(\sigma^{*2}-r)^2}$. The right hand side is positive for $r < \frac{\sigma^{*2}}{3}$.

Putting the pieces together, $\nu = \min \left\{ \left(\frac{1}{(\alpha^*+r)^2} \vee 1 \right), \frac{\sigma^{*2}-r}{2(\sigma^{*2}+r)^3} - \frac{(1-\alpha^*)r}{(\sigma^{*2}-r)^2}, \frac{1-\alpha^*}{\sigma^{*2}+r} - \frac{(1-\alpha^*)r}{(\sigma^{*2}-r)^2} \right\}$.

C2) The second condition is Lipschitz smoothness, which is stated in terms of $f = -q$ as follow:

$$f(\theta_1) - f(\theta_2) - \langle \nabla f(\theta_2), \theta_1 - \theta_2 \rangle \leq \frac{L}{2} \|\theta_1 - \theta_2\|_2^2.$$

In order to prove this condition, we start by introducing and demonstrating the following lemma.

Lemma 1.1. *If f is twice continuously differentiable, and $-\nabla^2 f + LI$ is positive semidefinite, with I the identity matrix, then f satisfied Lipschitz smoothness condition.*

Lemma 1.1. Note that Lipschitz smoothness condition is equivalent to:

$$(\nabla f(\theta_1) - \nabla f(\theta_2))^T (\theta_1 - \theta_2) \leq L \|\theta_1 - \theta_2\|_2^2.$$

Then the proof of the lemma follows as an adaptation of the proposition B.5 in Bertsekas (1995). Assume that $-\nabla^2 f(\theta) + LI$ is positive semidefinite, then for all $a \in \mathbb{R}^d$, $a^T (\nabla^2 f(\theta) - LI) a \leq 0$. Let $g : \mathbb{R} \rightarrow \mathbb{R}$ given as

$$g(t) = \nabla f(t\theta_1 + (1-t)\theta_2)^T (\theta_1 - \theta_2).$$

Using the mean value theorem, we have

$$(\nabla f(\theta_1) - \nabla f(\theta_2))^T(\theta_1 - \theta_2) = g(1) - g(0) = \frac{\partial g}{\partial t}(t^*)$$

for some $t^* \in [0, 1]$. Finally, we have

$$\frac{\partial g}{\partial t}(t^*) = (\theta_1 - \theta_2)^T \nabla^2 f(t\theta_1 + (1-t)\theta_2)^T(\theta_1 - \theta_2) \leq L \|\theta_1 - \theta_2\|_2^2$$

where the last inequality follows from the positive semi-definiteness of $-\nabla^2 f(\theta) + LI$. \square

By Lemma 1.1, if $-\nabla^2 f + LI$ is positive semidefinite, then Lipschitz smoothness condition is met. Now,

$$\begin{aligned} -\nabla^2 f(\theta) + LI &= \begin{bmatrix} -\left(\frac{\alpha^*}{\alpha^2} + \frac{1-\alpha^*}{(1-\alpha)^2}\right) + L & 0 & 0 \\ 0 & -\frac{1-\alpha^*}{\sigma^2} + L & -\frac{(1-\alpha^*)(\mu^*-\mu)}{\sigma^4} \\ 0 & -\frac{(1-\alpha^*)(\mu^*-\mu)}{\sigma^4} & -\left(-\frac{1}{2\sigma^4} + \frac{\sigma^{*2}}{\sigma^6}\right) + L \end{bmatrix} \\ &= \begin{bmatrix} m & 0 & 0 \\ 0 & n & p \\ 0 & p & q \end{bmatrix}. \end{aligned}$$

As before, we need to seek an $L > 0$ such that all of the principal minors are nonnegative, i.e. we need to ensure:

(a) $m \geq 0$.

This is satisfied if $L \geq \frac{\alpha^*}{(\alpha^*-r \vee 0.7)^2} + \frac{1-\alpha^*}{(1-\alpha^*-r \vee \omega)^2}$, where ω is a small positive constant;

(b) $n \geq 0$.

This is satisfied if $L \geq \frac{1-\alpha^*}{\sigma^{*2}-r}$;

(c) $q \geq 0$.

Note that

$$\sup_{\sigma^2 \in \mathbb{B}_2(r; \sigma^{*2})} \left[-\frac{1}{2\sigma^4} + \frac{\sigma^{*2}}{\sigma^6} \right] = \frac{\sigma^{*2} + r}{2(\sigma^{*2} - r)^3}, \text{ if } r < \sigma^{*2}.$$

Thus, the condition is satisfied if $L \geq \frac{\sigma^{*2} + r}{2(\sigma^{*2} - r)^3}$.

(d) $nq \geq p^2$.

Assuming that $\frac{\sigma^{*2}+r}{2(\sigma^{*2}-r)^3} < \frac{1-\alpha^*}{\sigma^{*2}-r}$, the left hand side of this last condition is bounded from below by $\left(L - \frac{1-\alpha^*}{\sigma^{*2}-r}\right)^2$. The right hand side is bounded from above by $\frac{(1-\alpha^*)^2r^2}{(\sigma^{*2}-r)^4}$. $L \geq \frac{(1-\alpha^*)\sigma^{*2}}{(\sigma^{*2}-r)^2}$ then satisfies condition (d). On the other hand, if $\frac{\sigma^{*2}+r}{2(\sigma^{*2}-r)^3} > \frac{1-\alpha^*}{\sigma^{*2}-r}$, by similar reasoning, take $L \geq \frac{\sigma^{*2}+r}{2(\sigma^{*2}-r)^3} + \frac{1-\alpha^*}{\sigma^{*2}-r}$.

Putting everything together, $L = \max \left\{ \frac{\alpha^*}{(\alpha^*-r \vee 0.7)^2} + \frac{1-\alpha^*}{(1-\alpha^*-r \vee \omega)^2}, \frac{(1-\alpha^*)\sigma^{*2}}{(\sigma^{*2}-r)^2}, \frac{\sigma^{*2}+r}{2(\sigma^{*2}-r)^3} + \frac{1-\alpha^*}{\sigma^{*2}-r} \right\}$

C3) The third condition is gradient smoothness: there exists an appropriately small parameter $\gamma \geq 0$, such that:

$$\|\nabla q(\theta) - \nabla Q(\theta|\theta)\|_2 \leq \gamma \|\theta - \theta^*\|_2$$

Recall that the data is generated according to g_{θ^*} , that is, $\xi \sim g_{\theta^*}$, where

$$g_{\theta}(\xi) = \alpha\phi(\xi; 0, \sigma^2) + (1-\alpha)\phi(\xi; \mu, \sigma^2)$$

and $\theta = (\alpha, \mu, \sigma^2)^T$. Denote as before $A = A_{\theta} := \alpha\phi(\xi; 0, \sigma^2)$ and $B = B_{\theta} := (1-\alpha)\phi(\xi; \mu, \sigma^2)$. Then we derive:

$$\begin{aligned} \nabla q(\theta) = \frac{\partial q(\theta)}{\partial \theta} = \frac{\partial Q(\theta|\theta^*)}{\partial \theta} = \mathbb{E} \left\{ \frac{1}{A^* + B^*} \left(A^* \frac{1}{\alpha} - B^* \frac{1}{1-\alpha} \right), \right. \\ \frac{B^*}{A^* + B^*} \frac{\xi - \mu}{\sigma^2}, \\ \left. \frac{A^*}{A^* + B^*} \left(-\frac{1}{2\sigma^2} + \frac{\xi^2}{2\sigma^4} \right) + \frac{B^*}{A^* + B^*} \left(-\frac{1}{2\sigma^2} + \frac{(\xi - \mu)^2}{2\sigma^4} \right) \right\} \end{aligned}$$

With a similar computation for $Q(\theta|\theta)$ we obtain

$$\begin{aligned} \nabla q(\theta) - \nabla Q(\theta|\theta) = \mathbb{E} \left\{ \left(\frac{A^*}{A^* + B^*} - \frac{A}{A + B} \right) \frac{1}{\alpha} - \left(\frac{B^*}{A^* + B^*} - \frac{B}{A + B} \right) \frac{1}{1-\alpha}, \right. \\ \left(\frac{B^*}{A^* + B^*} - \frac{B}{A + B} \right) \frac{\xi - \mu}{\sigma^2}, \\ \left(\frac{A^*}{A^* + B^*} - \frac{A}{A + B} \right) \left(-\frac{1}{2\sigma^2} + \frac{\xi^2}{2\sigma^4} \right) \\ \left. + \left(\frac{B^*}{A^* + B^*} - \frac{B}{A + B} \right) \left(-\frac{1}{2\sigma^2} + \frac{(\xi - \mu)^2}{2\sigma^4} \right) \right\}. \end{aligned}$$

Let $w = \frac{A^*}{A^*+B^*} - \frac{A}{A+B}$ and note that $-w = \frac{B^*}{A^*+B^*} - \frac{B}{A+B}$. Then we obtain

$$\begin{aligned}\nabla q(\theta) - \nabla Q(\theta|\theta) &= \mathbb{E} \left\{ w \frac{1}{\alpha(1-\alpha)}, w \frac{\mu-\xi}{\sigma^2}, w \frac{2\xi\mu-\mu^2}{2\sigma^4} \right\}^T \\ &= \mathbb{E} \left\{ -w \cdot \begin{bmatrix} 0 & -\frac{1}{\alpha(1-\alpha)} \\ \frac{1}{\sigma^2} & -\frac{\mu}{\sigma^2} \\ -\frac{\mu}{\sigma^4} & \frac{\mu^2}{2\sigma^4} \end{bmatrix} \cdot \begin{bmatrix} \xi \\ 1 \end{bmatrix} \right\}.\end{aligned}$$

The term $-w = \frac{A}{A+B} - \frac{A^*}{A^*+B^*} = w(\theta; \xi) - w(\theta^*; \xi)$. Taylor theorem for multivariate function gives:

$$-w = w(\theta; \xi) - w(\theta^*; \xi) = \sum_{i=1}^3 \left(\int_0^1 \nabla_i w(\theta_u; \xi) du \right) (\theta - \theta^*)_i \quad (1)$$

where $\nabla_i w(\theta_u; \xi) = \frac{\partial w(\theta; \xi)}{\partial \theta_i} |_{\theta=\theta_u}$ and $\theta_u = \theta^* + u(\theta - \theta^*)$ for $u \in [0, 1]$.

We have

$$\begin{aligned}\nabla w(\theta_u; \xi) &= \left\{ \frac{A_u B_u}{(A_u + B_u)^2} \frac{1}{\alpha_u(1-\alpha_u)}, \frac{A_u B_u}{(A_u + B_u)^2} \frac{\xi - \mu_u}{\sigma_u^2}, \frac{A_u B_u}{(A_u + B_u)^2} \frac{2\xi\mu_u - \mu_u^2}{2\sigma_u^4} \right\}^T \\ &= -\frac{A_u B_u}{(A_u + B_u)^2} \begin{bmatrix} 0 & -\frac{1}{\alpha_u(1-\alpha_u)} \\ \frac{1}{\sigma_u^2} & -\frac{\mu_u}{\sigma_u^2} \\ -\frac{\mu_u}{\sigma_u^4} & \frac{\mu_u^2}{2\sigma_u^4} \end{bmatrix} \begin{bmatrix} \xi \\ 1 \end{bmatrix}.\end{aligned} \quad (2)$$

Thus

$$\begin{aligned}\nabla q(\theta) - \nabla Q(\theta|\theta) &= \mathbb{E} \left\{ \begin{bmatrix} 0 & -\frac{1}{\alpha(1-\alpha)} \\ \frac{1}{\sigma^2} & -\frac{\mu}{\sigma^2} \\ -\frac{\mu}{\sigma^4} & \frac{\mu^2}{2\sigma^4} \end{bmatrix} \begin{bmatrix} \xi \\ 1 \end{bmatrix} \begin{bmatrix} \xi & 1 \end{bmatrix} \int_0^1 \frac{-A_u B_u}{(A_u + B_u)^2} \begin{bmatrix} 0 & -\frac{1}{\alpha_u(1-\alpha_u)} \\ \frac{1}{\sigma_u^2} & -\frac{\mu_u}{\sigma_u^2} \\ -\frac{\mu_u}{\sigma_u^4} & \frac{\mu_u^2}{2\sigma_u^4} \end{bmatrix} du (\theta - \theta^*) \right\} \\ &= \mathbb{E} \left\{ M \begin{bmatrix} \xi \\ 1 \end{bmatrix} \begin{bmatrix} \xi & 1 \end{bmatrix} \int_0^1 \frac{-A_u B_u}{(A_u + B_u)^2} M_u^T du (\theta - \theta^*) \right\}.\end{aligned}$$

Thus

$$\begin{aligned}
\|\nabla q(\theta) - \nabla Q(\theta|\theta)\|_2 &= \left\| \mathbb{E} \left\{ M \begin{bmatrix} \xi \\ 1 \end{bmatrix} \begin{bmatrix} \xi & 1 \end{bmatrix} \int_0^1 \frac{-A_u B_u}{(A_u + B_u)^2} M_u^T du (\theta - \theta^*) \right\} \right\|_2 \\
&= \left\| \int_0^1 \mathbb{E} \left\{ M \begin{bmatrix} \xi \\ 1 \end{bmatrix} \begin{bmatrix} \xi & 1 \end{bmatrix} \frac{-A_u B_u}{(A_u + B_u)^2} M_u^T du \right\} (\theta - \theta^*) \right\|_2 \\
&\leq \sup_{u \in [0,1]} \left\| \mathbb{E} \left\{ M \frac{-A_u B_u}{(A_u + B_u)^2} \begin{bmatrix} \xi \\ 1 \end{bmatrix} \begin{bmatrix} \xi & 1 \end{bmatrix} M_u^T \right\} \right\|_{op} \|\theta - \theta^*\|_2 \\
&\leq \sup_{u \in [0,1]} \left\| M \mathbb{E} \left\{ \frac{-A_u B_u}{(A_u + B_u)^2} \begin{bmatrix} \xi \\ 1 \end{bmatrix} \begin{bmatrix} \xi & 1 \end{bmatrix} \right\} M_u^T \right\|_F \|\theta - \theta^*\|_2 \\
&\leq \|M\|_F \sup_{u \in [0,1]} \left\| \mathbb{E} \left\{ \frac{-A_u B_u}{(A_u + B_u)^2} \begin{bmatrix} \xi^2 & \xi \\ \xi & 1 \end{bmatrix} \right\} \right\|_F \|M_u\|_F \|\theta - \theta^*\|_2. \\
\end{aligned} \tag{3}$$

The scheme is to bound $\mathbb{E} \left\{ \frac{A_u B_u \xi^2}{(A_u + B_u)^2} \right\}$, $\mathbb{E} \left\{ \frac{A_u B_u \xi}{(A_u + B_u)^2} \right\}$, $\mathbb{E} \left\{ \frac{A_u B_u}{(A_u + B_u)^2} \right\}$ appropriately, so that the terms in front of $\|\theta - \theta^*\|_2$ is appropriately small, or goes to 0 quickly as the signal (in a sense to be clarified later) becomes large.

First, we bound $\mathbb{E} \left\{ \frac{A_u B_u}{(A_u + B_u)^2} \right\}$. It can be checked that

$$\begin{aligned}
\sup_{\xi \in \mathbb{R}} \frac{A_u B_u}{(A_u + B_u)^2} &= \frac{A_u B_u}{(A_u + B_u)^2} \Big|_{\xi = \frac{\mu_u}{2} + \frac{\sigma_u^2}{\mu_u} \log(\frac{\alpha_u}{1-\alpha_u})} = \frac{1}{4} \\
\sup_{\xi \leq t_1} \frac{A_u B_u}{(A_u + B_u)^2} &= \frac{A_u B_u}{(A_u + B_u)^2} \Big|_{\xi = t_1}, \text{ for all } t_1 < \frac{\mu_u}{2} \\
\sup_{\xi \geq t_2} \frac{A_u B_u}{(A_u + B_u)^2} &= \frac{A_u B_u}{(A_u + B_u)^2} \Big|_{\xi = t_2}, \text{ for all } t_2 > \frac{\mu_u}{2} + \frac{\sigma_u^2}{\mu_u} \log \left(\frac{\alpha_u}{1-\alpha_u} \right).
\end{aligned}$$

Now,

$$\begin{aligned}
\mathbb{E} \left\{ \frac{A_u B_u}{(A_u + B_u)^2} \middle| \xi \geq t_2 \right\} &\leq \mathbb{E} \left\{ \frac{1}{\frac{A_u}{B_u} + \frac{B_u}{A_u} + 2} \middle| \xi = t_2 \right\} \\
&= \frac{1}{\frac{A_u}{B_u} + \frac{B_u}{A_u} + 2} \bigg|_{\xi = t_2} \\
&= \frac{1}{\frac{\alpha_u}{1-\alpha_u} \exp\left(-\frac{t_2^2}{2\sigma_u^2} + \frac{(t_2 - \mu_u)^2}{2\sigma_u^2}\right) + \frac{1-\alpha_u}{\alpha_u} \exp\left(\frac{t_2^2}{2\sigma_u^2} - \frac{(t_2 - \mu_u)^2}{2\sigma_u^2}\right) + 2} \\
&\leq \frac{1}{\frac{1-\alpha_u}{\alpha_u} \exp\left(\frac{t_2^2}{2\sigma_u^2} - \frac{(t_2 - \mu_u)^2}{2\sigma_u^2}\right)} = \frac{\alpha_u}{1-\alpha_u} \exp\left[\frac{\mu_u(\frac{\mu_u}{2} - t_2)}{\sigma_u^2}\right].
\end{aligned}$$

Similarly,

$$\begin{aligned}
\mathbb{E} \left\{ \frac{A_u B_u}{(A_u + B_u)^2} \middle| \xi \leq t_1 \right\} &\leq \mathbb{E} \left\{ \frac{1}{\frac{A_u}{B_u} + \frac{B_u}{A_u} + 2} \middle| \xi = t_1 \right\} \\
&= \frac{1}{\frac{A_u}{B_u} + \frac{B_u}{A_u} + 2} \bigg|_{\xi = t_1} \\
&= \frac{1}{\frac{\alpha_u}{1-\alpha_u} \exp\left(-\frac{t_1^2}{2\sigma_u^2} + \frac{(t_1 - \mu_u)^2}{2\sigma_u^2}\right) + \frac{1-\alpha_u}{\alpha_u} \exp\left(\frac{t_1^2}{2\sigma_u^2} - \frac{(t_1 - \mu_u)^2}{2\sigma_u^2}\right) + 2} \\
&\leq \frac{1}{\frac{1-\alpha_u}{\alpha_u} \exp\left(-\frac{t_1^2}{2\sigma_u^2} + \frac{(t_1 - \mu_u)^2}{2\sigma_u^2}\right)} = \frac{1-\alpha_u}{\alpha_u} \exp\left[\frac{\mu_u(t_1 - \frac{\mu_u}{2})}{\sigma_u^2}\right].
\end{aligned}$$

Thus, we can bound $\mathbb{E} \left\{ \frac{A_u B_u}{(A_u + B_u)^2} \right\}$ as follow:

$$\begin{aligned}
&\mathbb{E} \left\{ \frac{A_u B_u}{(A_u + B_u)^2} \right\} \\
&\leq \mathbb{E} \left\{ \frac{A_u B_u}{(A_u + B_u)^2} \middle| \xi \leq t_1 \right\} + \mathbb{E} \left\{ \frac{A_u B_u}{(A_u + B_u)^2} \middle| \xi \geq t_2 \right\} + \mathbb{E} \left\{ \frac{A_u B_u}{(A_u + B_u)^2} \middle| t_1 \leq \xi \leq t_2 \right\} \mathbb{P}(t_1 \leq \xi \leq t_2) \\
&\leq \frac{1-\alpha_u}{\alpha_u} \exp\left[\frac{\mu_u(t_1 - \frac{\mu_u}{2})}{\sigma_u^2}\right] + \frac{\alpha_u}{1-\alpha_u} \exp\left[\frac{\mu_u(\frac{\mu_u}{2} - t_2)}{\sigma_u^2}\right] + \frac{1}{4} \mathbb{P}(t_1 \leq \xi \leq t_2). \tag{4}
\end{aligned}$$

Let $t_2 = \frac{\mu_u}{2} + \frac{\sigma_u^2}{\mu_u} \log\left(\frac{\alpha_u}{1-\alpha_u}\right) + \omega_0 = \frac{\mu_u}{2} + \omega$, where ω_0 is a fixed small constant, and

$t_1 = \frac{\mu_u}{2} - \omega$. Then, assuming $\omega < \frac{\mu_u}{2}$, $\frac{\mu_u}{2} < \mu^* - \omega$ and $r < \mu^* - 2\omega$, we have:

$$\begin{aligned}
\mathbb{P}(t_1 \leq \xi \leq t_2) &= \alpha^* \mathbb{P}(t_1 \leq \xi_0 \leq t_2) + (1 - \alpha^*) \mathbb{P}(t_1 \leq \xi_1 \leq t_2) \\
&\quad \text{where } \xi_0 \sim N(0, \sigma^{*2}) \text{ and } \xi_1 \sim N(\mu^*, \sigma^{*2}) \\
&\leq \alpha^* \mathbb{P}\left(\xi_0 > \frac{\mu_u}{2} - \omega\right) + (1 - \alpha^*) \mathbb{P}\left(\xi_1 < \frac{\mu_u}{2} + \omega\right) \\
&\leq \alpha^* \phi^c\left(\frac{\frac{\mu_u}{2} - \omega}{\sigma^*}\right) + (1 - \alpha^*) \phi^c\left(\frac{\mu^* - \frac{\mu_u}{2} - \omega}{\sigma^*}\right) \\
&\leq \alpha^* \frac{1}{\sqrt{2\pi}} \frac{\sigma^*}{\frac{\mu_u}{2} - \omega} \exp\left[-\frac{1}{2\sigma^{*2}} \left(\frac{\mu_u}{2} - \omega\right)^2\right] \\
&\quad + (1 - \alpha^*) \frac{1}{\sqrt{2\pi}} \frac{\sigma^*}{\mu^* - \frac{\mu_u}{2} - \omega} \exp\left[-\frac{1}{2\sigma^{*2}} \left(\mu^* - \frac{\mu_u}{2} - \omega\right)^2\right] \\
&\leq \alpha^* \frac{1}{\sqrt{2\pi}} \frac{\sigma^*}{\frac{\mu^* - r}{2} - \omega} \exp\left[-\frac{1}{2\sigma^{*2}} \left(\frac{\mu^* - r}{2} - \omega\right)^2\right] \\
&\quad + (1 - \alpha^*) \frac{1}{\sqrt{2\pi}} \frac{\sigma^*}{\mu^* - \frac{\mu^* + r}{2} - \omega} \exp\left[-\frac{1}{2\sigma^{*2}} \left(\mu^* - \frac{\mu^* + r}{2} - \omega\right)^2\right] \\
&= \frac{1}{\sqrt{2\pi}} \frac{\sigma^*}{\frac{\mu^*}{2} - \frac{r}{2} - \omega} \exp\left[-\frac{1}{2\sigma^{*2}} \left(\frac{\mu^*}{2} - \frac{r}{2} - \omega\right)^2\right] \\
&= \frac{1}{\sqrt{2\pi}} \exp\left[-\log\left(\frac{\frac{\mu^*}{2} - \frac{r}{2} - \omega}{\sigma^*}\right) - \frac{1}{2} \left(\frac{\frac{\mu^*}{2} - \frac{r}{2} - \omega}{\sigma^*}\right)^2\right]. \tag{5}
\end{aligned}$$

Similarly,

$$\begin{aligned}
\frac{1 - \alpha_u}{\alpha_u} \exp\left[\frac{\mu_u(t_1 - \frac{\mu_u}{2})}{\sigma_u^2}\right] &\leq \frac{1 - \alpha_u}{\alpha_u} \exp\left[\frac{\mu_u(-\frac{\sigma_u^2}{\mu_u} \log(\frac{\alpha_u}{1 - \alpha_u}) - \omega_0)}{\sigma_u^2}\right] \\
&= \frac{1 - \alpha_u}{\alpha_u} \exp\left[-\log\left(\frac{\alpha_u}{1 - \alpha_u}\right) - \frac{\mu_u}{\sigma_u^2} \omega_0\right] \\
&= \left(\frac{1 - \alpha_u}{\alpha_u}\right)^2 \exp\left(-\frac{\mu_u}{\sigma_u^2} \omega_0\right) \\
&< \exp\left(-\frac{\mu^* - r}{\sigma^{*2} + r} \omega_0\right) \tag{6}
\end{aligned}$$

and

$$\frac{\alpha_u}{1 - \alpha_u} \exp\left[\frac{\mu_u(\frac{\mu_u}{2} - t_2)}{\sigma_u^2}\right] < \exp\left(-\frac{\mu^* - r}{\sigma^{*2} + r} \omega_0\right). \tag{7}$$

Combining equations (4), (5), (6) and (7), we have that for appropriately large μ^*

$$\begin{aligned} \mathbb{E} \left\{ \frac{A_u B_u}{(A_u + B_u)^2} \right\} &\leq 2 \exp \left(-\frac{\mu^* - r}{\sigma^{*2} + r} \omega_0 \right) + \frac{1}{\sqrt{2\pi}} \exp \left[-\log \left(\frac{\frac{\mu^*}{2} - \frac{r}{2} - \omega}{\sigma^*} \right) - \frac{1}{2} \left(\frac{\frac{\mu^*}{2} - \frac{r}{2} - \omega}{\sigma^*} \right)^2 \right] \\ &< C \exp \left(-\frac{\mu^* - r}{\sigma^{*2} + r} \omega_0 \right). \end{aligned} \quad (8)$$

Now, we bound $\mathbb{E} \left\{ \frac{A_u B_u}{(A_u + B_u)^2} \xi^2 \right\}$ as follow:

$$\begin{aligned} \mathbb{E} \left\{ \frac{A_u B_u}{(A_u + B_u)^2} \xi^2 \right\} &\leq \mathbb{E} \left\{ \frac{A_u B_u}{(A_u + B_u)^2} \xi^2 \middle| \xi \leq t_1 \right\} + \mathbb{E} \left\{ \frac{A_u B_u}{(A_u + B_u)^2} \xi^2 \middle| \xi \geq t_2 \right\} \\ &\quad + \mathbb{E} \left\{ \frac{A_u B_u}{(A_u + B_u)^2} \xi^2 \middle| t_1 \leq \xi \leq t_2 \right\} \mathbb{P}(t_1 \leq \xi \leq t_2) \\ &\leq \sup_{\xi \leq t_1} \frac{A_u B_u}{(A_u + B_u)^2} \mathbb{E}(\xi^2) + \sup_{\xi \geq t_2} \frac{A_u B_u}{(A_u + B_u)^2} \mathbb{E}(\xi^2) \\ &\quad + \frac{1}{4} \mathbb{E}(\xi^2) \mathbb{P}(t_1 \leq \xi \leq t_2) \\ &< C \exp \left(-\frac{\mu^* - r}{\sigma^{*2} + r} \omega_0 \right) (\sigma^{*2} + (1 - \alpha^*)\mu^*). \end{aligned} \quad (9)$$

Lastly, from (8) and (9) we have

$$\begin{aligned} \mathbb{E} \left\{ \frac{A_u B_u \xi}{(A_u + B_u)^2} \right\} &= \mathbb{E} \left\{ \frac{\sqrt{A_u B_u}}{A_u + B_u} \frac{\sqrt{A_u B_u} \xi}{A_u + B_u} \right\} \leq \sqrt{\mathbb{E} \left\{ \frac{A_u B_u}{(A_u + B_u)^2} \right\}} \sqrt{\mathbb{E} \left\{ \frac{A_u B_u \xi^2}{(A_u + B_u)^2} \right\}} \\ &< C \exp \left(-\frac{\mu^* - r}{\sigma^{*2} + r} \omega_0 \right) \sqrt{\sigma^{*2} + (1 - \alpha^*)\mu^*} \end{aligned} \quad (10)$$

where the first inequality follows from the classic Cauchy-Schwarz inequality.

Putting everything together, and noting that the terms $\|M\|_2$ and $\|M_u\|_2$ in (3) are polynomial in μ^* and σ^{*2} , we conclude that:

$$\|\nabla q(\theta) - \nabla Q(\theta|\theta)\|_2 \leq \gamma(\alpha^*, \mu^*, \sigma^{*2}) \|\theta - \theta^*\|_2 \quad (11)$$

where $\gamma(\alpha^*, \mu^*, \sigma^{*2}) \sim O \left(\frac{\mu^{*5}}{\sigma^{*8}} \exp(-\frac{\mu^* - r}{\sigma^{*2} + r} \omega_0) \right)$ goes to 0 exponentially fast with large $\frac{\mu^*}{\sigma^{*2}}$. \square

S1.2 Proof of Proposition 4.2

Proof. Let $w(\theta; \xi) = \frac{A_\theta}{A_\theta + B_\theta}$, where $A_\theta := \alpha\phi(\xi; 0, \sigma^2)$ and $B_\theta := (1 - \alpha)\phi(\xi; \mu, \sigma^2)$. We obtain

$$\sup_{\theta \in \mathbb{B}_2(r; \theta^*)} \|\nabla Q_n(\theta | \theta) - \nabla Q(\theta | \theta)\|_2 = \sup_{\theta \in \mathbb{B}_2(r; \theta^*)} \|\mathbf{R}(\theta)\mathbf{x}\|_2 \leq \sup_{\theta \in \mathbb{B}_2(r; \theta^*)} \|\mathbf{R}(\theta)\|_{op} \|\mathbf{x}\|_2$$

where

$$\mathbf{R}(\theta) = \begin{bmatrix} 0 & 0 & \frac{1}{\alpha(1-\alpha)} & 0 \\ \frac{1}{\sigma^2} & 0 & \frac{\mu}{\sigma^2} & \frac{-1}{\sigma^2} \\ \frac{-\mu}{\sigma^4} & \frac{1}{2\sigma^4} & \frac{\mu^2}{2\sigma^4} & \frac{\mu}{\sigma^4} \end{bmatrix} \text{ and } \mathbf{x} = \begin{pmatrix} \frac{1}{n} \sum_{i=1}^n \xi_i - \mathbb{E}(\xi) \\ \frac{1}{n} \sum_{i=1}^n \xi_i^2 - \mathbb{E}(\xi^2) \\ \frac{1}{n} \sum_{i=1}^n w(\theta; \xi_i) - \mathbb{E}(w(\theta; \xi)) \\ \frac{1}{n} \sum_{i=1}^n w(\theta; \xi_i) \xi_i - \mathbb{E}(w(\theta; \xi) \xi) \end{pmatrix}.$$

The elements of the column vector \mathbf{x} can be regarded as empirical processes and can be bound separately. The first 2 elements do not involve θ , and thus by SLLN,

$$P \left(\left| \frac{1}{n} \sum_{i=1}^n \xi_i - \mathbb{E}(\xi) \right| > \omega \right) \rightarrow 0 \text{ almost surely, as } n \rightarrow \infty.$$

Similarly

$$P \left(\left| \frac{1}{n} \sum_{i=1}^n \xi_i^2 - \mathbb{E}(\xi^2) \right| > \omega \right) \rightarrow 0 \text{ almost surely, as } n \rightarrow \infty.$$

To bound the remaining 2 elements, we use covering number. The following definition and theorem correspond to Definition 23 and Theorem 24 from Pollard (1984).

Definition 1.1 (Pollard, 1984). *Let P be a probability measure on ξ , \mathcal{F} be a class of function in $\mathcal{L}^1(P)$. For each $\omega > 0$, define the covering number $N(\omega, P, \mathcal{F})$ as the smallest value of m for which there exists functions g_1, \dots, g_m such that $\min_j \mathbb{E}_P |f - g_j| \leq \omega$ for each $f \in \mathcal{F}$. Set $N(\omega, P, \mathcal{F}) = \infty$ if no such m exists.*

Theorem 1.2 (Pollard, 1984). *Let \mathcal{F} be a class of function with envelope F integrable with respect to P . If P_n is obtained by independent sampling from the probability measure P and if $\log N(\omega, P_n, \mathcal{F}) = o_p(n)$ for each fixed $\omega > 0$, then $\sup_{\mathcal{F}} |\mathbb{E}_{P_n} f - \mathbb{E}_P f| \rightarrow 0$ almost surely.*

Let $\mathcal{F}_1 = \{w(\theta; \xi) : \theta \in \mathbb{B}_2(r; \theta^*)\}$, and $\mathcal{F}_2 = \{w(\theta; \xi)\xi : \theta \in \mathbb{B}_2(r; \theta^*)\}$. Then $F_1(\xi) = 1$ an envelope of \mathcal{F}_1 , and $F_2(\xi) = |\xi|$ an envelope of \mathcal{F}_2 ; F_1, F_2 are integrable.

We set out to prove that $\log N(\omega, P_n, \mathcal{F}_1) = o_p(n)$ and $\log N(\omega, P_n, \mathcal{F}_2) = o_p(n)$.

Similar to (1) and (2), letting $\theta_u = \theta_2 + u(\theta_1 - \theta_2)$, we have

$$\begin{aligned}
P_n |w(\theta_1; \xi) - w(\theta_2; \xi)| &= \frac{1}{n} \sum_{i=1}^n |w(\theta_1; \xi_i) - w(\theta_2; \xi_i)| \\
&= \frac{1}{n} \sum_{i=1}^n \left| \int_0^1 -\frac{A_u B_u}{(A_u + B_u)^2} [\xi_i \ 1] \begin{bmatrix} 0 & -\frac{1}{\alpha_u(1-\alpha_u)} \\ \frac{1}{\sigma_u^2} & -\frac{\mu_u}{\sigma_u^2} \\ -\frac{\mu_u}{\sigma_u^4} & \frac{\mu_u^2}{2\sigma_u^4} \end{bmatrix}^T du (\theta_1 - \theta_2) \right| \\
&\leq \frac{1}{n} \sum_{i=1}^n \left| \sup_{u \in [0,1]} -\frac{A_u B_u}{(A_u + B_u)^2} [\xi_i \ 1] M_u^T (\theta_1 - \theta_2) \right| \text{ where } M_u \text{ is the above matrix} \\
&\leq \frac{1}{n} \sum_{i=1}^n \sup_{u \in [0,1]} \left\| \frac{A_u B_u}{(A_u + B_u)^2} [\xi_i \ 1] \right\|_2 \|M_u\|_{op} \|\theta_1 - \theta_2\|_2 \\
&\leq \frac{1}{n} \sum_{i=1}^n \sup_{u \in [0,1]} \left\| \frac{A_u B_u}{(A_u + B_u)^2} [\xi_i \ 1] \right\|_2 \|M_u\|_F \|\theta_1 - \theta_2\|_2.
\end{aligned}$$

We note that θ_1, θ_2 and θ_u are in $\mathbb{B}_2(r; \theta^*)$, and thus $\|M_u\|_F$ can be bounded by a constant $M(\theta^*; r) \in \mathbb{R}$, and this constant is of order a polynomial of elements in θ^* .

Letting $D = \frac{1}{n} \sum_{i=1}^n \sup_{u \in [0,1]} \left\| \frac{A_u B_u}{(A_u + B_u)^2} [\xi_i \ 1] \right\|_2 M(\theta^*; r)$, then $\|\theta_1 - \theta_2\|_2 < \frac{\omega}{D}$ implies $P_n |w(\theta_1; \xi) - w(\theta_2; \xi)| < \omega$. This means $N(\omega, P_n, \mathcal{F}_1) \leq N(\frac{\omega}{D}, \|\cdot\|_2, \mathbb{B}_2(r; \theta^*)) \leq (1 + \frac{2rD}{\omega})^3$, where the last inequality is due to proposition 4.2.12, Vershynin (2018), or can be proved by comparing volumes of corresponding balls in \mathbb{R}^3 . Thus, our task now becomes

proving that $3 \log(1 + \frac{2rD}{\omega}) = o_p(n)$. Let δ be any positive constant, then

$$\begin{aligned}
P \left\{ 3 \log \left(1 + \frac{2rD}{\omega} \right) > n\delta \right\} &= P \left\{ D > \frac{(e^{n\delta/3} - 1)\omega}{2r} \right\} \\
&= P \left\{ \frac{1}{n} \sum_{i=1}^n \sup_{u \in [0,1]} \left\| \frac{A_u B_u}{(A_u + B_u)^2} [\xi_i \ 1] \right\|_2 M(\theta^*; r) > \frac{(e^{n\delta/3} - 1)\omega}{2r} \right\} \\
&\leq P \left\{ \frac{1}{n} \sum_{i=1}^n \sup_{u \in [0,1]} \left\| \frac{A_u B_u}{(A_u + B_u)^2} [\xi_i \ 1] \right\|_2 > \frac{(e^{n\delta/3} - 1)\omega}{2r M(\theta^*; r)} \right\} \\
&\leq P \left\{ \max_{\xi_i} \sup_{u \in [0,1]} \left\| \frac{A_u B_u}{(A_u + B_u)^2} [\xi_i \ 1] \right\|_2 > \frac{(e^{n\delta/3} - 1)\omega}{2r M(\theta^*; r)} \right\} \\
&\leq n P \left\{ \sup_{u \in [0,1]} \left\| \frac{A_u B_u}{(A_u + B_u)^2} [\xi \ 1] \right\|_2 > \frac{(e^{n\delta/3} - 1)\omega}{2r M(\theta^*; r)} \right\} \\
&\leq n P \left\{ \sup_{u \in [0,1]} \frac{A_u B_u |\xi|}{(A_u + B_u)^2} + \frac{A_u B_u}{(A_u + B_u)^2} > \frac{(e^{n\delta/3} - 1)\omega}{2r M(\theta^*; r)} \right\} \\
&\leq n P \left\{ \sup_{u \in [0,1]} \frac{A_u B_u |\xi|}{(A_u + B_u)^2} > \frac{(e^{n\delta/3} - 1)\omega}{4r M(\theta^*; r)} \right\} \\
&\quad + n P \left\{ \sup_{u \in [0,1]} \frac{A_u B_u}{(A_u + B_u)^2} > \frac{(e^{n\delta/3} - 1)\omega}{4r M(\theta^*; r)} \right\} \\
&\leq n \mathbb{E} \left\{ \sup_{u \in [0,1]} \frac{A_u B_u |\xi|}{(A_u + B_u)^2} \right\} \frac{4r M(\theta^*; r)}{(e^{n\delta/3} - 1)\omega} \tag{12}
\end{aligned}$$

$$+ n \mathbb{E} \left\{ \sup_{u \in [0,1]} \frac{A_u B_u}{(A_u + B_u)^2} \right\} \frac{4r M(\theta^*; r)}{(e^{n\delta/3} - 1)\omega} \tag{13}$$

where the last inequality is by a Markov inequality. Note that in (8) and (10), the bounds for $\mathbb{E} \left\{ \frac{A_u B_u}{(A_u + B_u)^2} \right\}$ and $\mathbb{E} \left\{ \frac{A_u B_u \xi}{(A_u + B_u)^2} \right\}$ work the same as $\mathbb{E} \left\{ \sup_{u \in [0,1]} \frac{A_u B_u}{(A_u + B_u)^2} \right\}$ and $\mathbb{E} \left\{ \sup_{u \in [0,1]} \frac{A_u B_u |\xi|}{(A_u + B_u)^2} \right\}$ Thus, (12) can be bounded

$$\begin{aligned}
P \left\{ 3 \log \left(1 + \frac{2rD}{\omega} \right) > n\delta \right\} &\leq C \exp \left(-\frac{\mu^* - r}{\sigma^{*2} + r} \omega_0 \right) \sqrt{\sigma^{*2} + (1 - \alpha^*)\mu^*} \frac{4nr M(\theta^*; r)}{(e^{n\delta/3} - 1)\omega} \\
&\quad + C \exp \left(-\frac{\mu^* - r}{\sigma^{*2} + r} \omega_0 \right) \frac{4nr M(\theta^*; r)}{(e^{n\delta/3} - 1)\omega} \rightarrow 0 \text{ as } n \rightarrow \infty. \tag{14}
\end{aligned}$$

Thus, the case for $N(\omega, P_n, \mathcal{F}_1)$ is proved. For $N(\omega, P_n, \mathcal{F}_2)$, we proceed similarly:

$$\begin{aligned}
P_n |w(\theta_1; \xi)\xi - w(\theta_2; \xi)\xi| &= \frac{1}{n} \sum_{i=1}^n |w(\theta_1; \xi_i)\xi_i - w(\theta_2; \xi_i)\xi_i| \\
&= \frac{1}{n} \sum_{i=1}^n \left| \int_0^1 -\frac{A_u B_u}{(A_u + B_u)^2} [\xi_i^2 \ \xi_i] \begin{bmatrix} 0 & -\frac{1}{\alpha_u(1-\alpha_u)} \\ \frac{1}{\sigma_u^2} & -\frac{\mu_u}{\sigma_u^2} \\ -\frac{\mu_u}{\sigma_u^4} & \frac{\mu_u^2}{2\sigma_u^4} \end{bmatrix}^T du (\theta_1 - \theta_2) \right| \\
&\leq \frac{1}{n} \sum_{i=1}^n \sup_{u \in [0,1]} \left\| \frac{A_u B_u}{(A_u + B_u)^2} [\xi_i^2 \ \xi_i] \right\|_2 \|M_u\|_F \|\theta_1 - \theta_2\|_2.
\end{aligned}$$

Replacing D with $\frac{1}{n} \sum_{i=1}^n \sup_{u \in [0,1]} \left\| \frac{A_u B_u}{(A_u + B_u)^2} [\xi_i^2 \ \xi_i] \right\|_2 M(\theta^*; r)$, then $N(\omega, P_n, \mathcal{F}_2) \leq N(\frac{\omega}{D}, \|\cdot\|_2, \mathbb{B}_2(r; \theta^*)) \leq (1 + \frac{2rD}{\omega})^3$, and as before

$$\begin{aligned}
P \left\{ 3 \log \left(1 + \frac{2rD}{\omega} \right) > n\delta \right\} &= P \left\{ D > \frac{(e^{n\delta/3} - 1)\omega}{2r} \right\} \\
&\leq n \mathbb{E} \left\{ \sup_{u \in [0,1]} \frac{A_u B_u \xi^2}{(A_u + B_u)^2} \right\} \frac{4rM(\theta^*; r)}{(e^{n\delta/3} - 1)\omega} \\
&\quad + n \mathbb{E} \left\{ \sup_{u \in [0,1]} \frac{A_u B_u |\xi|}{(A_u + B_u)^2} \right\} \frac{4rM(\theta^*; r)}{(e^{n\delta/3} - 1)\omega} \\
&\leq C \exp \left(-\frac{\mu^* - r}{\sigma^{*2} + r} \omega_0 \right) \left(\sigma^{*2} + (1 - \alpha^*)\mu^* \right) \frac{4nrM(\theta^*; r)}{(e^{n\delta/3} - 1)\omega} \\
&\quad + C \exp \left(-\frac{\mu^* - r}{\sigma^{*2} + r} \omega_0 \right) \sqrt{\sigma^{*2} + (1 - \alpha^*)\mu^*} \frac{4nrM(\theta^*; r)}{(e^{n\delta/3} - 1)\omega}
\end{aligned} \tag{15}$$

$\rightarrow 0$ as $n \rightarrow \infty$.

□

S2 Additional Figures

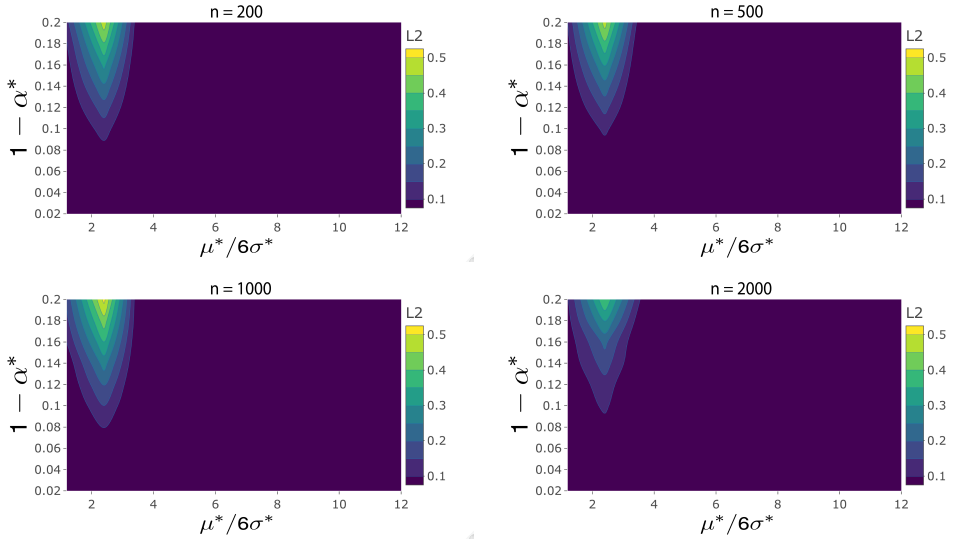


Figure S1. (from left to right, top to bottom) L2-error of smooth component estimate in the case of 'clumped' spikes when $n = 200$, $n = 500$, $n = 1000$, $n = 2000$.

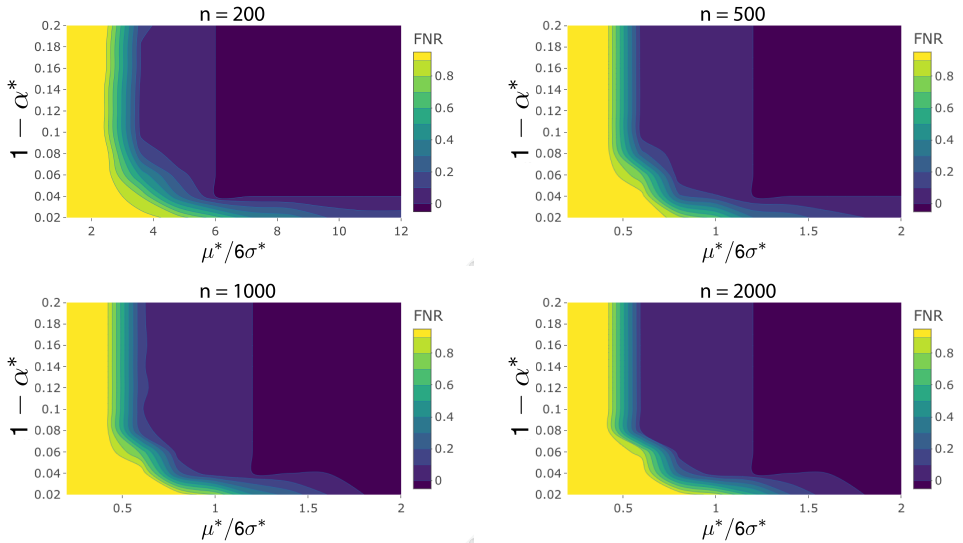


Figure S2. (from left to right, top to bottom) FNR of spikes identification in the case of 'clumped' spikes when $n = 200$, $n = 500$, $n = 1000$, $n = 2000$.

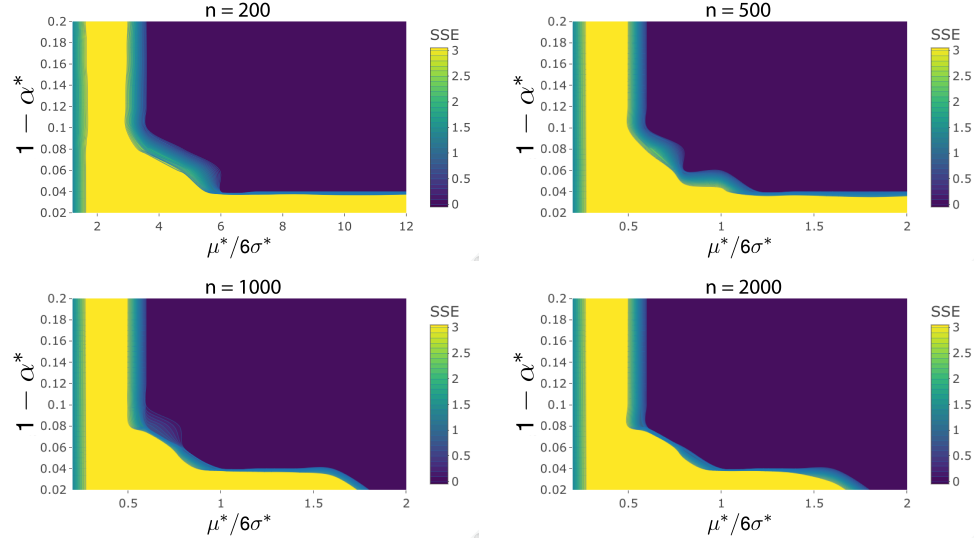


Figure S3. (from left to right, top to bottom) SSE of parameter estimates in the case of 'clumped' spikes when $n = 200$, $n = 500$, $n = 1000$, $n = 2000$.

References

Balakrishnan, S., Wainwright, M. J. and Yu, B. (2017) Statistical guarantees for the EM algorithm: from population to sample-based analysis. *The Annals of Statistics*, **45**, 77–120.

Bertsekas, D. P. (1995) *Nonlinear Programming*. Athena Scientific.

Pollard, D. (1984) *Convergence of stochastic processes*. Springer-Verlag.

Vershynin, R. (2018) *High-dimensional probability*. Cambridge University Press.